ISSN 0024-4902, Lithology and Mineral Resources, 2024, Vol. 59, No. 1, pp. 47–69. © Pleiades Publishing, Ltd., 2024.

Cretaceous–Eocene Flysch of the Sochi Synclinorium (Western Caucasus): Sources of Clastic Material Based on the Results of U–Th–Pb Isotope Dating of Detrital Zircons

N. B. Kuznetsov[a, *], T. V. Romanyuk[b], A. V. Shatsillo[b], I. V. Latysheva[a], I. V. Fedyukin[b], A. V. Strashko[a], A. S. Novikova[a], E. A. Shcherbinina[a], A. V. Drazdova[a], E. I. Makhinya[a], A. V. Marinin[b], A. S. Dubenskiy[a, c], K. G. Erofeeva[a, d], and V. S. Sheshukov[a]

[a] *Geological Institute, Russian Academy of Sciences (GIN RAS), Moscow, 119017 Russia*

[b] *Schmidt Institute of Physics of the Earth, Russian Academy of Sciences, Moscow, 123242 Russia*

[c] *Faculty of Chemistry, Lomonosov Moscow State University, Moscow, 119991 Russia*

[d] *Institute of Geology of Ore Deposits, Petrography, Mineralogy and Geochemistry, Russian Academy of Sciences, Moscow, 119017 Russia*

**e-mail: kouznikbor@mail.ru*

Received July 12, 2023; revised August 17, 2023; accepted September 4, 2023

Abstract—The first results of the U–Th–Pb isotope dating of detrital zircons (dZr, N = 130, $n = 91$) from the middle Danian sandstones (63.9–65.3 Ma) of the Cretaceous–Eocene Novorossiisk–Anapa flysch widely developed in the Sochi synclinorium (southern slope of the Western Caucasus) are presented. The maximum and minimum dZr age is 2973 ± 12 Ma and 318 ± 3 Ma, respectively; weighted average age of the four youngest dZr is ~322 ± 7 Ma. There are no signs of erosion products of the Jurassic magmatites involved in the structure of the Greater Caucasus and Crimean Mountains into the sedimentary basin, where the Novorossiisk–Anapa flysch was formed. The results have revealed a high degree of similarity between the provenance signals of the Danian sandstones from the Novorossiisk–Anapa flysch, some Paleogene–Neogene and Early Quaternary (Early Pleistocene) sandstones of the Western Caucasus and Western Cis-Caucasia, red-colored Upper Permian and Lower Triassic sandstones of the Moscow syneclise, as well as Late Quaternary alluvium at lower reaches of the Don and Volga rivers draining vast expanses of the Russian Plate. These facts suggest: (1) the absence of eroded mountain structures of the Greater Caucasus and Crimea in the middle Danian; (2) the main volume of detrital material composing the Novorossiisk–Anapa flysch was formed due to the recycling of Permian–Triassic and younger sequences of the Russian Plate.

Keywords: Sochi synclinorium, Paleocene, sandstones, zircon, U–Pb dating, provenances, paleogeography

DOI: 10.1134/S0024490223700384

INTRODUCTION

Despite the long history of geological and geophysical study of the Black Sea–Balkan–Anatolian–Caucasian (BSBAC) region (Fig. 1) and the abundance of accumulated materials, there are still significant gaps in unraveling the geodynamics of Greater Caucasus orogen formation and the accompanying change of paleogeographic settings in adjacent regions. As shown in numerous paleogeographic and paleotectonic reconstructions for the end-Mesozoic (Nikishin et al., 2015a, 2015b, 2015c; Okay and Nikishin, 2015; Wilhelm, 2014a, 2014b), the region, which included the present-day Cis-Caucasia along with northern parts of the Black Sea and Caspian Sea represented a part of the northern periphery of the Tethys Ocean that separated the Arctic–Laurasian and Gondwanan continental masses.

Due to the closure of the Tethys Ocean and the convergence of continental masses, the northern BSBAC region became in the Cenozoic a part of the spacious epicontinental basin (defined as Peri-Tethys) in the Cenozoic and represented a complex system of sub-basins connected by narrow straits. The vanishing of straits connecting the sub-basins led to episodic interruptions of the link of sub-basins with the Mediterranean sector of the World Ocean, abrupt changes in the hydrological regime, catastrophic drops in sea level, and replacement of the marine faunal communities by the freshwater species and so on. A sharp weakening of water exchange with the ocean in the Oligocene led to the formation of a semi-enclosed Para-Tethys Basin (Palcu et al., 2021; Popov et al., 2004, 2009, 2010).

In our work, parts of the Peri-Tethys and Para-Tethys, located on the site of present-day Crimea and

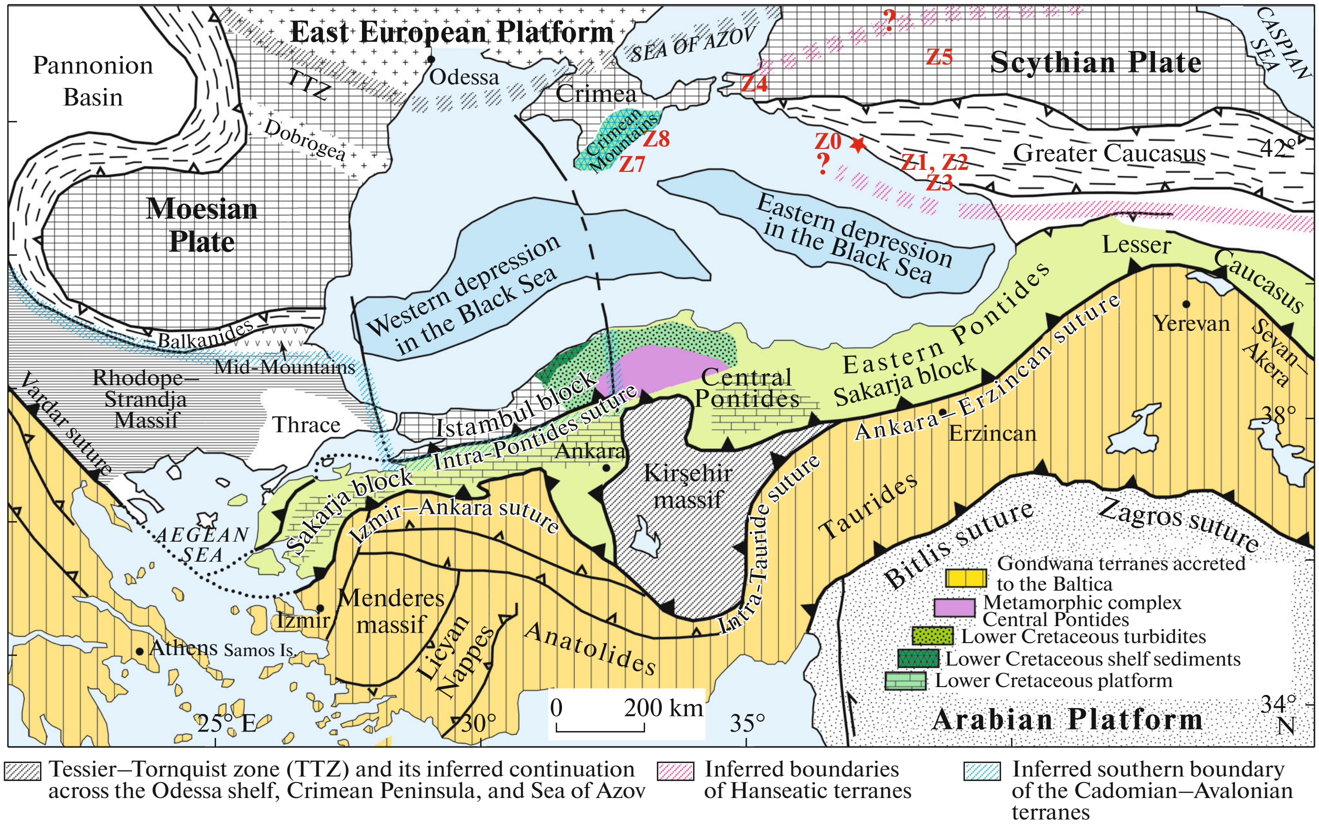

Fig. 1. Tectonic scheme of the Black Sea–Balkan–Anatolian megaregion. Based on (Okay et al., 2001) and modified after (Okay et al., 2013). The red asterisk and mark **Z0** denote the sample K21–012 site in the Novorossiisk–Anapa flysch. Red marks **Z1–Z8** indicate the position of regions or sampling sites, with the U–Pb dating results of detritus zircon grains discussed in the text and shown in Figs. 8 and 9.

the Caucasus, are defined as the Crimean–Caucasian sedimentary basin. Some sequences formed in this basin are exposed currently in the Crimean Mountains, on both slopes of the Greater Caucasus, and in the southern (close to the Greater Caucasus) part of the Cis-Caucasus. In addition, these sequences are drilled by numerous boreholes in the Cis-Caucasian trough and characterized by seismostratigraphic materials (Popov et al., 2004, 2010). Analysis of the accumulated geological and geophysical materials made it possible to carry out the paleotectonic and paleogeographic reconstructions reported in (Afanasenkov et al., 2007; *Bol'shoi Kavkaz* ..., 2007; Nikishin et al., 2010; Vincent et al., 2007, 2013 and references therein). These reconstructions show that the part of the Crimean–Caucasian Basin, where the Greater Caucasus is located now, accommodated a deep-water trough in the Late Mesozoic–Early Cenozoic. Then, the deformation of rocks in this trough began not earlier than the Oligocene, followed by uplift of the Greater Caucasus. At the same time, Oligocene–Quaternary foredeeps (Tuapse and West Kuban) were formed on both sides of the western segment of the Greater Caucasus uplift.

Since the Western Cis-Caucasus and, in particular, the West Kuban trough, is an oil-bearing area, its sedimentary infill has already been studied well by seismic exploration methods and drilling. Specific details of the seismostratigraphic sections characterizing the sedimentary infill in the West Kuban trough indicate clearly that, during the Late Mesozoic and almost entire Cenozoic (up to Early Pleistocene included), the basin was filled with sediments mainly due to the clinoforms (Patina and Popov, 2023; Popov et al., 2010). Because of such basin infill mechanism, there is no doubt that they were transported into the West Kuban trough or basin (at least, its northern part) mainly from the northern platform-type structures—young (epi-Hercynian) Scythian Platform and ancient East European Platform (EEP). Relatively small thicknesses of the Upper Pliocene–Quaternary layers in the West Kuban trough hinder the identification of clinoforms, different-rank erosion boundaries, paleoincisions, and other structural elements that can suggest the sedimentation flow direction.

The Cis-Caucasian part of the Tuapse trough is strongly deformed (Almendinger et al., 2011; Baskakova et al., 2022). Therefore, we cannot recognize in seismostratigraphic sections specific details that could make it possible to estimate the directions of sedimentation flows and predict the position of provenances of the detrital material.

Thus, the concept of paleotectonic and paleogeographic evolution of the Crimean–Caucasian sedimentary basin presented in (Afanasenkov et al., 2007; *Bol'shoi Kavkaz* ... ..., 2007; Nikishin et al., 2010; Vincent et al., 2007, 2013, and references there), is widely developed and recognized. Moreover, the Mesozoic–Cenozoic sedimentary sequences in the Greater Caucasus, Cis-Caucasus, and adjacent parts of the BSBAC region have been studied well by the conventional geological–geophysical methods. Neverthelss, many points of the Cenozoic regional paleotectonics and paleogeography mentioned below have not yet been resolved:

(1) Whether the Crimean–Caucasian sedimentary basin areas, where the Tuapse and West Kuban troughs are located now, were incorporated in a single basin with the same sources before the Middle Eocene, or they had already been separated by small uplifts (located at the site of the future Caucasus) prior to the uplift of the western segment of the Greater Caucasus? In other words, whether the above-mentioned areas represented a single Crimean–Caucasian sedimentary basin (including the present-day Tuapse and West Kuban troughs), individual sub-basins with various provenances, or foredeeps filled with erosion products of rock complexes and structures of the Western Caucasus?

(2) Is the Late Mesozoic–Cenozoic paleogeographic evolution of the western segment of the Greater Caucasus and the adjacent eastern and western regions, i.e., the central segment of the Greater Caucasus and Crimean Mountains, respectively, is different, and if so, in what way?

(3) Whether evolution history of the Crimean–Caucasian sedimentary basin was monotonous or it had certain time limits marked by a critical change in sedimentation conditions, sedimentation flow directions, provenances, and others?

To determine the provenances and solve many other regional paleogeographic issues, geologists have begun to apply in the last decade the bulk U–Th–Pb isotope dating of detritus zircon (dZr) grains from sedimentary rocks. The results of such studies provided insight into the age of crystal complexes (primary sources of dZr) and made it possible to: (1) determine the feeding provinces; and (2) reconstruct the directions of sedimentation flows filling the basins that accommodated the studied clastic rocks and others. Comparison of the obtained sets of dZr ages from detrital rocks of different sequences makes it possible to: (i) record changes in the provenances; (ii) obtain additional objective information for the paleotectonic and paleogeographic reconstructions; and (iii) solve the above-mentioned problems of regional geology and paleogeography.

To date, stratified different-age formations of the Greater Caucasus and Cis-Caucasus have already been characterized partially by the U–Th–Pb datings of dZr (Allen et al., 2006; Cowgill et al., 2016; ; Költringer et al., 2022; Mityukov et al., 2011; Tye et al.., 2021; Vasey et al., 2020; Vincent et al., 2013), but only two of these works (Mityukov et al., 2011; Vincent et al., 2013) characterize clastic rocks from the pre-Late Quaternary stratified sequences in the western segment of the Greater Caucasus and western regions of the Cis-Caucasus. However, most of the results presented in these works can now only be classified as preliminary (see DISCUSSION below).

In this article, we present new results of the U–Th–Pb dating of dZr in sandstones from the middle Danian part of the Novorossiisk–Anapa flysch section exposed in coastal cliffs of the Black Sea at the Kiselev Clift in the central Sochi synclinorium (southern slope of the Western Caucasus). We accomplished a comparative analysis and comparison of these results with the available similar data on the U–Th–Pb dating of dZr from different-age sandstones in the western segment of the Greater Caucasus, Crimean Mountains, and Moscow syneclise in the EEP.

GEOLOGICAL SETTING OF THE KISELEV CLIFT SEGMENT

Within the western segment of the Greater Caucasus, its southern slope accommodates the Sochi synclinorium, which is a relic of the Callovian–Miocene deep-water trough filled with the carbonate, terrigenous, terrigenous–carbonate, and clayey rocks (Afanasenkov et al., 2007). The Cenomanian–Eocene part of this sequence is marked by a flyschoid internal structure (*Geologiya* ..., 1968, p. 322). We identify this large element of the section in the northern and central parts of the Sochi synclinorium as the Novorossiisk–Anapa flysch.

The transverse section of the northern and central parts of the Sochi synclinorium is divided into several anticlinal and synclinal structures, including the Anapa–Agoi synclinal zone extending along the Black Sea coast. Within its limits, to the west of the meridian of Tuapse, the synclinal fold cores are composed of the uppermost elements (up to the Eocene and, possibly, the Lower Oligocene) of the composite Novorossiisk–Anapa flysch section (Fig. 2) (Marinin and Rastsvetaev, 2008; Marinin et al., 2017).

In the Black Sea coast section located between mouths of the Agoi and Tuapse rivers, the section and folded structure of the Novorossiisk–Anapa flysch is presented in a series of magnificent rock outcrops. We studied a fragment of the Novorossiisk–Anapa flysch section in the rock massif known as "Kiselev Clift" and in several adjacent coastal outcrops. Here, the

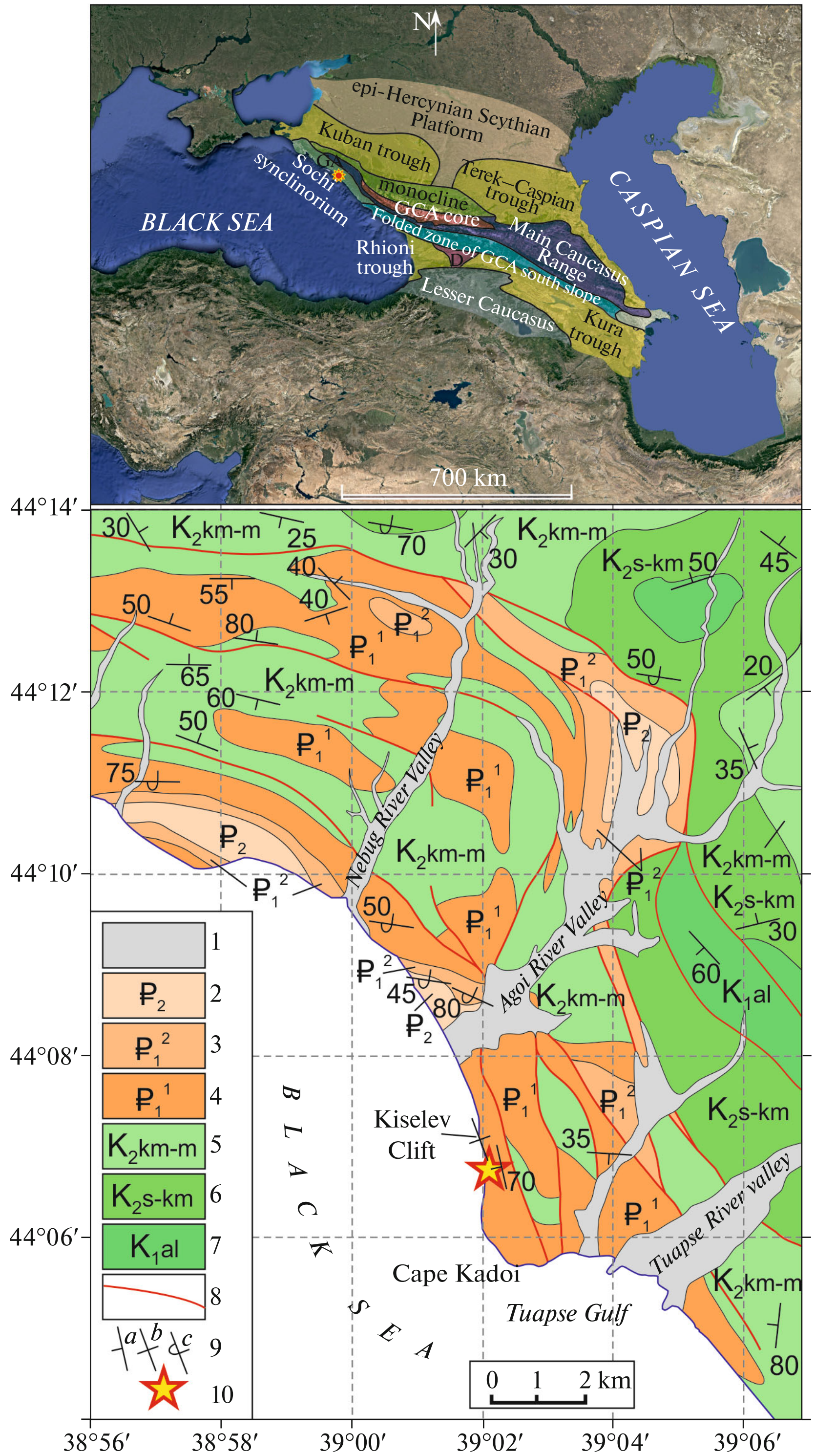

Fig. 2. Tectonic scheme of the Caucasus (above) and the schematic geological structure of the Nebug–Tuapse region (below). Based on (Korsakov et al., 2002, 2021; Marinin et al., 2017) and modified after our field studies. GCA—Great Caucasus anticlinorium, D—Dzirulla massif. (1–7) Fields of sequences: Quaternary—alluvial deposits (1), Eocene (2), Upper Paleocene (3), Lower Paleocene–Danian (4), Campanian–Maastrichtian (5), Cenomanian–Santonian (6), Albian (7); (8) fractures; (9) bedding patterns: inclined (*a*), vertical (*b*), overturned (*c*); (10) site of sample K21-012 in the Novorossiisk–Anapa flysch.

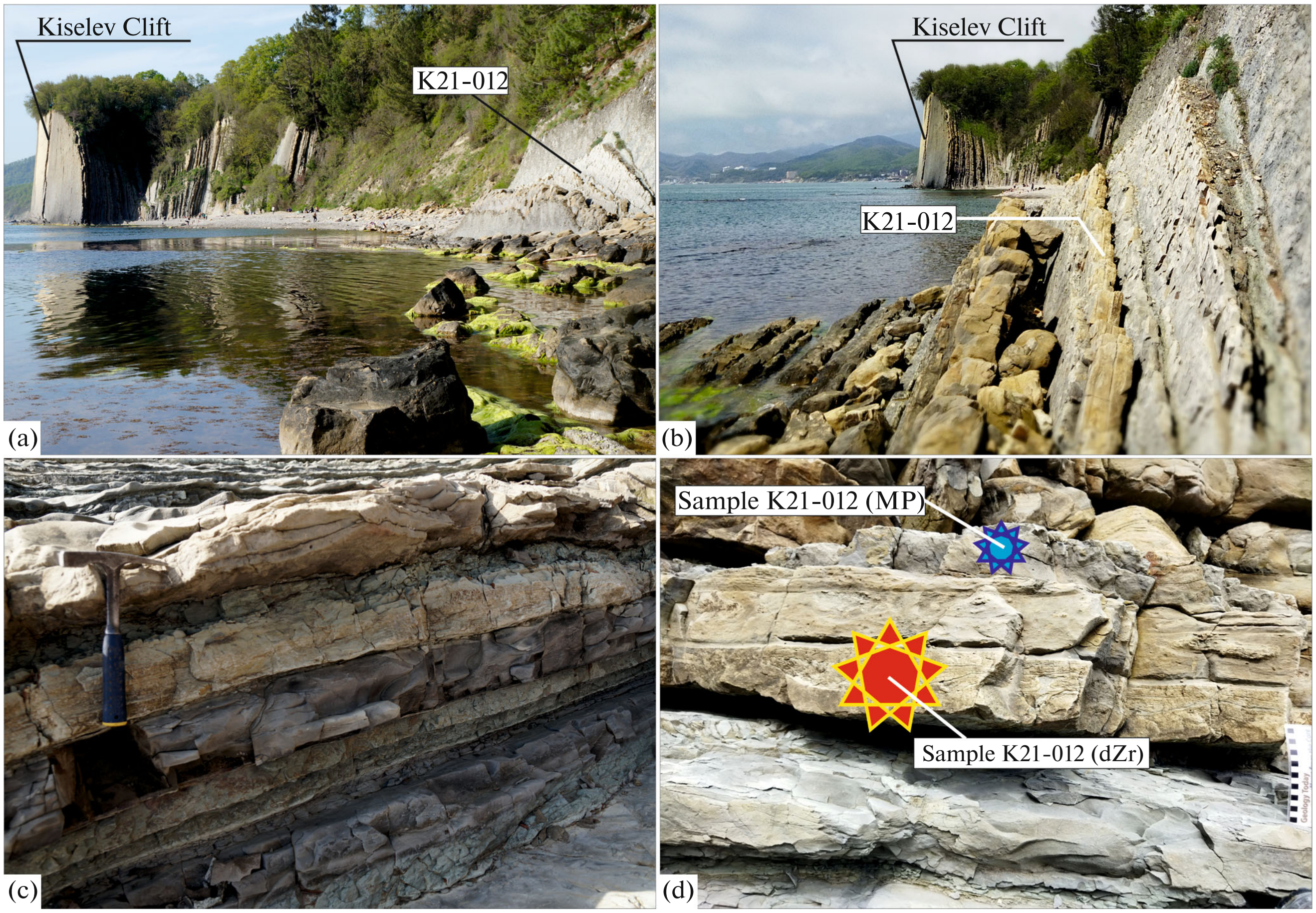

Fig. 3. General view and details of rock outcrops in the Novorossiisk–Anapa flysch located south of the Kiselev Clift. (a) Kiselev Clift (distant view) and rocks limiting the southward beach (view from the southern limit of this beach); (b) Kiselev Clift (medium view) and rock outcrop of the Novorossiisk–Anapa flysch (observation points K21-012, 44°06′36.83″ N 39°01′59.13″ E); (c) closeup of the structure of a vertical ledge in the southern framing of the beach located south of Kiselev Clift illustrating the distinctly rhythmic structure of the Novorossiisk–Anapa flysch; (d) one of the turbidite rhythms (incomplete Bouma Cycle) in the Novorossiisk–Anapa flysch fragment studied in Kiselev Clift, with the indication of sites of the detrital zircon sampling from sandstones at the turbidite rhythm base (sample K21-012 (dZr)) and the micropaleontological sampling of silty mudstones in the upper element of the same rhythm (sample K21-012 (MP)).

Novorossiisk–Anapa flysch is observed as a rhythmic alternation (Figs. 3a–3c) of calcareous sandstones, silty sandstones, siltstones, and clayey limestones. Thickness of individual (elementary) rhythms ranges from 20–30 cm (Fig. 3c) to 1 m or more in some places. The rhythms represent the typical Bouma Cycles (or Sequences) with elements designated by letters from “a” or “b” to “e” (Bouma, 1962; Shanmugam, 2021), with the only difference that element “e” is represented not by clayey rocks (mudstones), but by pelitomorphic clayey limestones. Boundaries of complete and incomplete rhythms, if their base is composed of sandstones (elements “a”, “b”, or even “c” of the Bouma Cycle), are often marked with abundant ichnofossils (Fig. 4a). The transverse surfaces of layers of these sandy rocks are marked by convolute stratification, which is obviously related to the dehydration of structures of the sandy sediment during its lithification (Figs. 4b, 4c). If the turbidite rhythms lack the Bouma Cycle elements composed of sandy rocks (elements “a”, “b”, and “c”), and the rhythm base includes silty rocks composing elements “d” and “e” of the Bouma Cycle, the boundaries of rhythms are marked by small flat-convex lenses of sandy rocks representing, apparently, cross-sections of small erosion channels in lateral parts of the distribution system of turbidite fans (Fig. 4d).

The Novorossiisk–Anapa flysch in many areas of its distribution (the Kiselev Clift section included) is characterized by a steep, vertical, and often overturned bedding. In most cases, it is easy to determine the top and bottom of individual layers in exposed clasts of the section using the following indicators: (1) presence of prominent graded layering; (2) presence of ichnofossils (casts of the traces of bottom organism crawling on the bottom of sandy rock layers (elements “a”, “b”, and “c” of the Bouma Cycle) forming the base of individual turbidite rhythms (Fig. 4a); (3) manifestation of

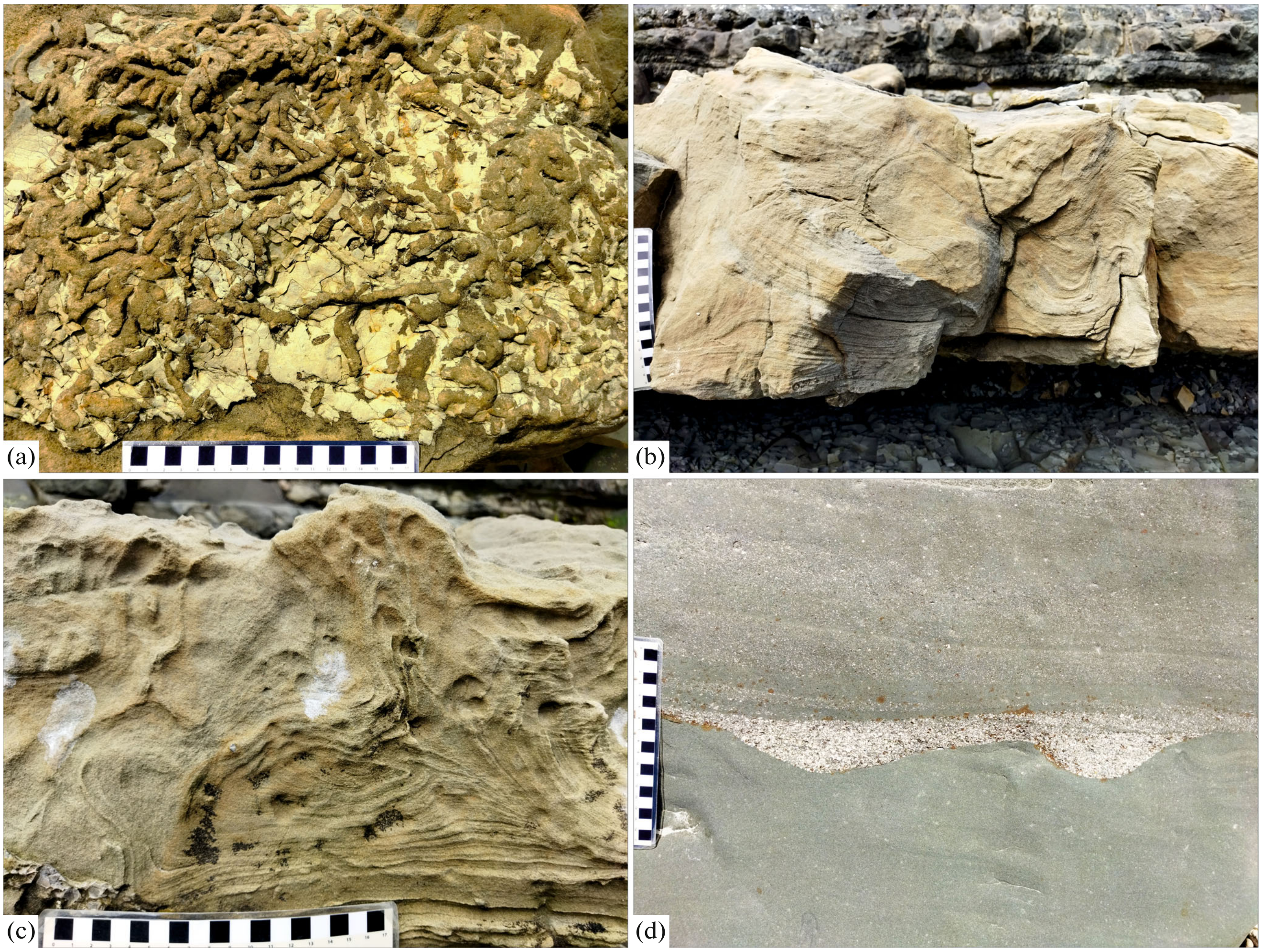

Fig. 4. Some features of the internal structure of the Novorossiisk–Anapa flysch fragment in the Kiselev Clift area. (a) Abundant ichnofossils (casts of the traces of bottom organism crawling) on the bottom of a sandstone layer at the turbidite rhythm base; (b, c) convolute layering in sandy rocks in turbidite rhythms; (d) erosion channels filled with sandy materials at the bottom of an incomplete rhythm represented by thin-layered rocks (elements “d” and “e” of the Bouma Cycle).

the convolute layering in sandy rocks (elements “a”, “b”, and “c” of the Bouma Cycle) (Figs. 4b, 4c); (4) presence of an cross-layered internal structure of sandy rocks (elements “c” of the Bouma Cycle); (5) presence of erosion channels filled with sandy material at the bottom of incomplete rhythms represented only by thin rocks composing elements “d” and “e” of the Bouma Cycle (Fig. 4d); and (6) combinations of all or parts of the listed structural features. Understanding the position of the section top and bottom allows us to decipher in the first approximation the complex fractured-folded structure of the Novorossiisk–Anapa flysch at the Kiselev Clift site (Fig. 2).

SAMPLING OF ROCKS AND THEIR DESCRIPTION

On the coastal cliff located 300 m south of the southern end of the rock massif known as Kiselev Clift (Figs. 2, 3a, 3b), we took sample K21-012 (about 3 kg) of the calcareous sandstone at the turbidite rhythm base at a point with coordinates 44°06′36.83″ N 39°01′59.13″ E (Fig. 3d).

The sandstones are light ash-gray, massive, fine- to medium-grained, and ocherous on the weathered surface. Microscopic examination of sandstones revealed that they are characterized by a clastic psammite texture. The poorly sorted, nonsorted, or mostly sharp-angled clasts (0.05–2 mm across) are represented mainly by quartz, with rare feldspars and detritus flakes of white mica. A significant part is composed of glauconite grains, bioclasts (clasts of carbonate shells, bryozoans, corals, and carbonate or siliceous formations), as well as intact foraminiferal shells of Lenticulina, Nodosaria, and Globigerina (Fig. 5). The detrital part (terrigenous clasts, glauconite, bioclasts and foraminiferal shells) makes up 50–60 vol %. The cement (40–50 vol %) is composed of a calcareous, solid, unevenly distributed basal and porous, fine- to microcrystalline (rarely, medium-crystalline and even coarse-crystalline) material. In the latter case, the cement is poikilitc.

The studied sample of light gray calcareous siltstone (Fig. 3d) is characterized by an extremely poor calcareous nannofossil assemblage. According to E.A. Shcherbinina (GIN RAS), the assemblage includes five species: *Braarudosphaera bigelowii* (Gran and Braarud) Deflandre, *Cruciplacolithus primus* Perch-Nielsen, *Prinsius dimorphosus* (Perch-Nielsen) Perch-Nielsen, small *Coccolithus pelagicus* (Wallich) Schiller, and calcite dinocysts *Cervisiella operculata* (Bramlette and Martini) Streng, Hildebrand-Habel and Williams. The presence of *P. dimorphosus* and the absence of younger species in this assemblage constrains the age range of embedding sediments to the lower part of the Danian—zone CNP3 (Agnini et al., 2014) or the upper part of zone NP2 and zone NP3 (Martini, 1971). According to GTS 2020 for the Paleogene Period (Speijer et al., 2020), this range corresponds to the absolute age of approximately 63.9–65.3 Ma.

PREPARATION OF SAMPLES, EXTRACTION OF ZIRCON CRYSTALS, AND THEIR CHARACTERISTICS

From sample K21-012 (about 3 kg), we took a part of the material (about 1.5 kg) that was crushed manually in a cast-iron mortar to a size class of –0.25 mm using a disposable nylon sieve. A pelitic and fine-aleuritic suspension (less than 20–30 μm) was extracted from the crushed material in the running tap water. Then, this material was dried in a fume hood and divided into the light and heavy fractions in a GPS-B heavy liquid (density ~2.9 g/cm^3). After washing the material from the heavy liquid remnants and drying in a fume hood, magnetic minerals were separated from the heavy mineral fraction using an electromagnetic separator at GIN RAS. The obtained heavy nonmagnetic mineral fraction contained numerous zircon grains. The zircon grains were not concentrated up to the monofraction level. The grains for analysis were randomly selected manually using a binocular microscope and were implanted into an epoxy mount using the standard methodological techniques.

Characteristics of zircon grains. All dZr grains from sample K21-012 implanted in the epoxy mount were studied at GIN RAS using an optical microscope, and some grains were examined on a TESCAN electron microscope in the cathode luminescence mode. The dZr grains (from 20–30 to 150–170 μm in size) display extremely diverse high interference colors in terms of luminescence intensity, color range, and interference spectrum (Fig. 6). The grains are represented mainly by the medium- to well-rounded crystals, with only a few grains retaining the elongated acicular shape. Some dZr grains have retained the features inherent in well-developed crystals. Most dZr grains represent either rounded parts of larger crystals or grains with initially intricate (up to amorphous) structure. They contain numerous inclusions of different nature. Sometimes, the inclusions are acicular (most likely, apatite crystals). Some dZr grains distinctly show cores with rims.

METHODS OF THE ANALYTICAL STUDY AND PRELIMINARY PROCESSING OF RESULTS

The U–Th–Pb isotope dating of zircon grains by the LA-ICP-MS method was performed at the Center for Collective Use of Equipment at GIN RAS. The laser microprobe analysis was accomplished using an LA NWR-213 system (Electro Scientific Ind.) combined with an Element 2 high-resolution magnetosector ICP mass spectrometer (Thermo Scientific Inc.). Operating parameters of the equipment are given in (Nikishin et al., 2020).

Isotope measurements were calibrated based on zircon GJ-1 (Elhlou et al., 2006; Jackson et al., 2004) as external standard. The quality of analyses was assessed by the sequential measurements in the control standards of zircon 91500 (Wiedenbeck et al., 1995, 2004; Yuan et al., 2008), Plesovice (Sláma et al., 2008), and unknown samples. The zircon standards GJ-1, 91500, and Plesovice yielded the following estimates of the weighted average concordant age (±2σ): 600.5 ± 1.5 (n = 59), 1073 ± 35 (n = 13), and 337.0 ± 2.1 (n = 13) Ma. Within the measurement error, these values are consistent with the $^{206}Pb/^{238}U$ isotope ratio-certified weighted average values of the CA-ID-TIMS age of these standards (±2σ): 601.9 ± 0.4 (n = 7), 1063.5 ± 0.4 (n = 7), and 337.2 ± 0.1 (n = 10) Ma (Horstwood et al., 2016).

Analytical results were processed using the commercial GLITTER (Griffin et al., 2008) and Isoplot/Ex (Ludwig, 2012) software packages. Theoretical corrections for the common Pb and calculation formulas are substantiated in (Andersen, 2002). The corrections were accomplished using the ComPbCorr software package (Andersen, 2008). Disturbance of the U–Th–Pb isotope system of zircon grains was estimated based on the measured contents of ^{206}Pb, ^{207}Pb, and ^{208}Pb in zircon and the known isotopic ratios between Pb isotopes, which are accepted in the program as $^{206}Pb/^{204}Pb = 18.7$, $^{207}Pb/^{204}Pb = 15.628$, $^{208}Pb/^{204}Pb = 38.63$.

To draw the bar chart and probability density curve (PDC), we used the analyses (conditional dating) satisfying the following three conditions: (1) $-10\% < D1$ and $D2 < 10\%$; (2) the analytical measurement error ensures the accuracy of age estimate <50 Ma; and (3) correction for the common Pb changes the age <50 Ma.

The GLITTER software package used for processing the primary analytical data makes it possible

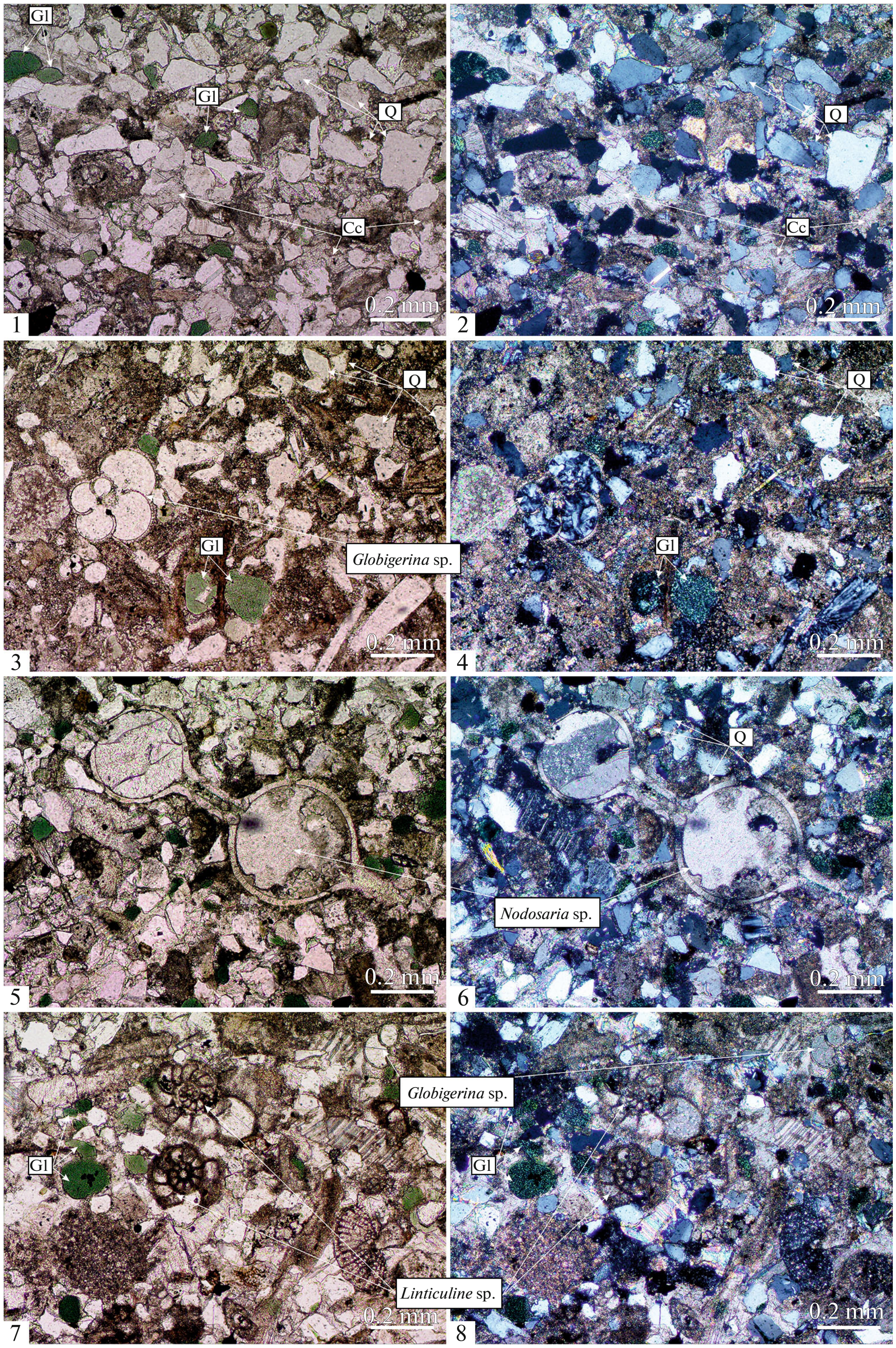

Fig. 5. Photomicrographs of thin sections of sandstones in sample K21-012. On the left: (1, 3, 5, 7) photomicrographs with parallel nicols; on the right: (2, 4, 6, 8) with crossed nicols. (1, 2) Sandstone enriched with quartz (Q) and glauconite (Gl), unsorted massive, with basal calcite cement (Cc); (3, 4) quartz sandstone (with glauconite), unsorted massive, with abundant calcite cement, numerous acicular carbonate and siliceous bodies (bioclasts), as well as intact shell of foraminifera Globigerina filled with silica (chalcedony); (5, 6) quartz-rich sandstone (with glauconite), unsorted massive, with the basal calcite cement and intact shell of foraminifera Nodosaria filled with crystalline carbonate (calcite); (7, 8) quartz-rich sandstone (with glauconite), unsorted massive, with abundant calcite cement, bioclasts, and intact shells of foraminifera Lenticulina.

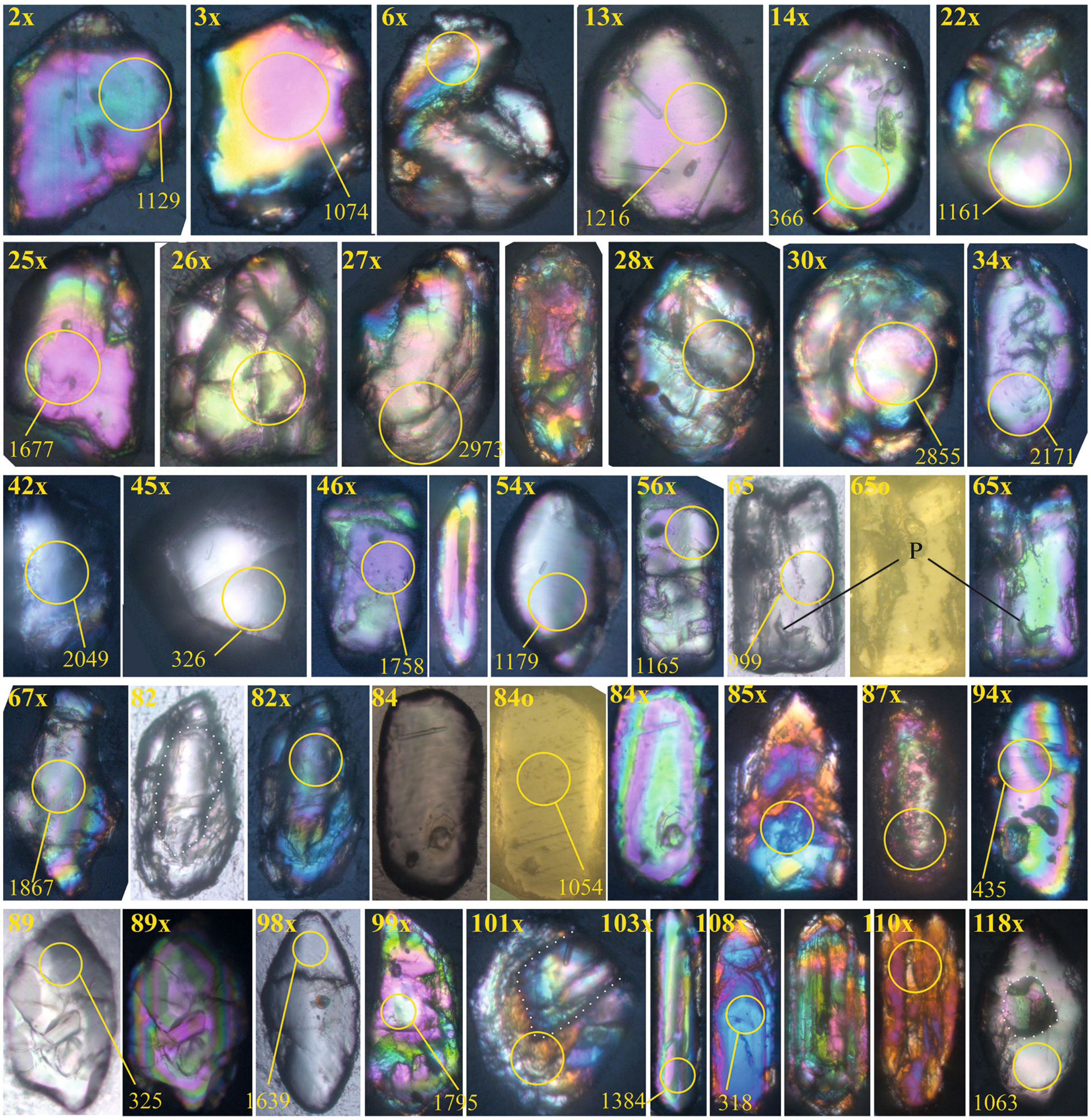

Fig. 6. Layout of optical images of the studied detrital zircon grains from sandstones of the Danian interval of the Novorossiisk–Anapa flysch section (sample K21-012). For each image, analysis number is indicated in the upper left corner (absent if sampling was not accomplished), index "o" means that the image was obtained in reflected light; without index, in transmitted light with parallel nicols; index "x", in transmitted light with crossed nicols. Some grains are furnished with two or three images. If the grain was probed, position of the laser ablation crater (circle, diameter 25 μm) and conditional age of the grain (in Ma) are shown. White dotted lines outline visible cores or boundaries between heterogeneous parts inside the grain. Three images without numbers are examples of grains with such a complex internal structure that they did not contain any area (25 μm across) without obvious distortions or inclusions and, therefore, hampered the U–Pb dating. Images 13, 14, 28, 34, 84, 94 89, 98, 118 and others are examples of grains with diverse inclusions. Three images of grain 65 in the transmitted and reflected light demonstrate an example of void space (P).

during each single isotope analysis to see a time sweep ("analytical signal") of the number of ions arriving at the ^{206}Pb, ^{207}Pb, ^{208}Pb, ^{232}Th, and ^{238}U recorders as the laser beam penetrates the investigated zircon grain and vaporizes the substance from the deeper parts of this grain. Different parts of the analytical signal correspond to different parts of the zircon grain. The GLITTER software package enables the researcher to "cut" any part of the received analytical signal, and thus obtain the isotopic date corresponding to different parts of the grain. Initial parts of the analytical signal correspond to a zircon grain sector located imme-

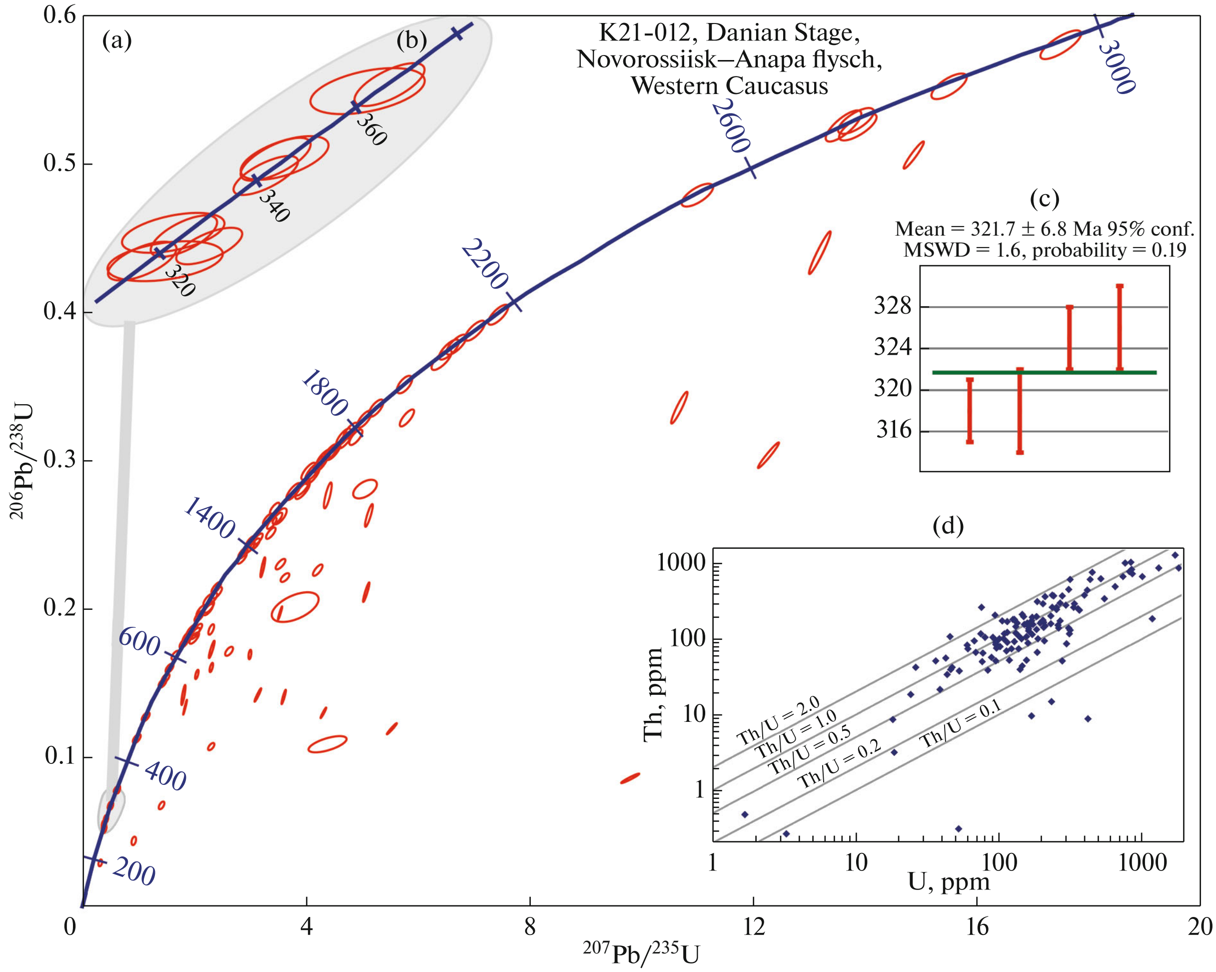

Fig. 7. Results of the study of the U–Th–Pb isotope system in detrital zircon grains from sample K21-012. (a) Diagram with concordia. Ellipses show the 68% confidence interval of measurements for all analyses (±1σ); (b) gray background shows an exaggerated concordia fragment; (c) diagram illustrating the weighted average age of 322 ± 7 Ma based on four youngest U–Pb datings; (d) diagram of the contents of Th and U. Analysis a55 (very low contents of U = 0.2 ppm and Th = 0.4 ppm) is not shown.

diately below its surface polished in the epoxy mount; the middle and end sectors, to the deeper (relative to the polished surface) parts of this grain. If the zircon grain in the analytical preparation is polished approximately to the middle sector, initial parts of the analytical signal most often correspond to the core; the end parts, to the zircon grain rim.

RESULTS

In sample K21-012, the U–Th–Pb isotope system was studied in 130 dZr grains. The obtained results are given in Table 1. In many of the analyzed dZr grains, the age was determined based on the analytical signal sector most likely corresponding to the grain core or rim labeled, respectively, as 'cor' and 'rim' in Table 1. The analytical record “a81" yielded two age estimates overlapping within the error limits: 1144 ± 18 (D1 = 0.0%, D2 = –0.1%); 1178 ± 18 (D1 = 3.2%, D2 = 9.4%). Analyses “a55” (very low contents of U = 0.2 ppm and Th = 0.4 ppm and, consequently, a large analytical error) and “a87” yielded noninterpretable values.

Age estimates of ~35% dZr grains are characterized by strong discordance (Fig. 7a), indicating a large-scale thermal (metamorphic) and/or metasomatic impact (possibly, repeated) on the analyzed dZr grains, resulting in the distortion of their U–Th–Pb isotope system to different (sometimes very significant) degrees (D > 30%). In the rocks, from which sample K21-012 was taken, no obvious traces of metamorphic or metasomatic alterations were revealed during their lithological and petrographic study. Therefore, it is most likely that the “discordant” dZr grains were recycled from rocks that had undergone the thermal (metamorphic) and/or metasomatic alterations.

In dZr grains from sandstones in the studied fragment of the Novorossiisk–Anapa flysch section, the content of U and Th varies, respectively, from 0.2 to

Table 1. Results of the U–Th–Pb isotopic (LA-ICP-MS) dating of detritus zircon grains from Danian sandstones of the Cretaceous–Paleocene Novorossiisk–Anapa flysch, widely developed in the Sochi synclinorium located on the southern slope of the western segment of the Greater Caucasus (sample K21-012)

Ord. no.	Analysis no. in sample	U, ppm	Th, ppm	Measured ratios (corrected for common Pb)						Age, Ma						D1, %	D2, %
				$^{207}Pb/^{206}Pb$	±1σ	$^{207}Pb/^{235}U$	±1σ	$^{206}Pb/^{238}U$	±1σ	$^{206}Pb/^{238}U$	±1σ	$^{207}Pb/^{235}U$	±1σ	$^{207}Pb/^{206}Pb$	±1σ		
1	a001-core	162.2	88.6	0.0948	0.00159	2.0435	0.01844	0.1563	0.00226	1525	18	1130	6	936	13	20.7	62.9
2	a002	232.0	204.6	0.0773	0.00105	1.9886	0.02578	0.1866	0.00185	**1129**	**16**	1112	9	1103	10	0.8	2.4
3	a003	114.8	70.4	0.0752	0.00118	1.8435	0.02772	0.1778	0.00183	**1074**	**18**	1061	10	1055	10	0.6	1.8
4	a004	146.2	100.7	0.0774	0.00111	2.0578	0.02834	0.1929	0.00194	**1131**	**17**	1135	9	1137	10	–0.2	–0.5
5	a005	124.2	74.5	0.1128	0.00162	4.9202	0.06769	0.3164	0.00324	**1845**	**15**	1806	12	1772	16	1.9	4.1
6	a006	175.0	156.3	0.1307	0.00215	3.5500	0.02698	0.1970	0.00299	2108	17	1538	6	1159	16	32.7	81.9
7	a007	279.9	374.9	0.1353	0.00198	4.2220	0.05929	0.2263	0.00234	2168	14	1678	12	1315	12	27.6	64.9
8	a008	139.3	75.2	0.0754	0.0011	1.9244	0.027	0.1851	0.00187	**1080**	**17**	1090	9	1095	10	–0.5	–1.4
9	a009	24.4	18.4	0.0932	0.00162	3.3434	0.05616	0.2603	0.00282	**1492**	**19**	1491	13	1491	14	0.0	0.1
10	a010	770.8	1026.2	0.2405	0.00448	4.3274	0.03004	0.1305	0.0023	3123	17	1699	6	791	13	114.8	294.8
11	a011-core	84.7	38.7	0.1110	0.00152	5.0176	0.06604	0.3277	0.00332	**1817**	**14**	1822	11	1827	16	–0.3	–0.5
12	a012-core	18.2	8.8	0.0934	0.00206	3.3595	0.07166	0.2610	0.00316	**1495**	**24**	1495	17	1495	16	0.0	0.0
13	a013-core	43.8	34.2	0.0808	0.00151	2.2718	0.04107	0.2040	0.00224	**1216**	**21**	1204	13	1197	12	0.6	1.6
14	a014	426.5	8.8	0.0539	0.00082	0.4347	0.00638	0.0585	0.00059	369	20	367	5	**366**	**4**	0.3	0.8
15	a015-core	189.1	102.1	0.0899	0.00132	2.3097	0.0327	0.1865	0.00191	1422	16	1215	10	1102	10	10.3	29.0
16	a016	106.7	175.0	0.2933	0.0053	12.2506	0.11199	0.3029	0.00499	3435	16	2624	9	1706	25	53.8	101.3
17	a018-core	92.2	106.2	0.0707	0.00186	1.4615	0.03716	0.1500	0.00186	947	31	915	15	**901**	**10**	1.6	5.1
18	a019-core	863.3	833.6	0.0544	0.00089	0.3843	0.00609	0.0512	0.00053	388	21	330	4	**322**	**3**	2.5	20.5
19	a020	45.9	107.1	0.1900	0.00269	13.8571	0.19029	0.5289	0.00545	**2742**	**14**	2740	13	2737	23	0.1	0.2
20	a021	95.6	90.3	0.0956	0.0013	3.5438	0.0464	0.2689	0.00272	**1540**	**15**	1537	10	1535	14	0.1	0.3
21	a022-center	126.0	182.8	0.0785	0.0012	2.1522	0.03167	0.1988	0.00205	**1161**	**17**	1166	10	1169	11	–0.3	–0.7
22	a023	297.4	280.5	0.1066	0.00136	4.5241	0.05547	0.3080	0.00305	**1741**	**14**	1735	10	1731	15	0.2	0.6
23	a024	76.5	263.2	0.0877	0.00133	2.8357	0.04131	0.2346	0.00242	**1375**	**17**	1365	11	1359	13	0.4	1.2
24	a025	115.7	169.3	0.1029	0.0015	4.1347	0.05797	0.2915	0.003	**1677**	**15**	1661	11	1649	15	0.7	1.7
25	a026	312.9	139.5	0.1596	0.00268	3.1379	0.02461	0.1426	0.0022	2451	16	1442	6	859	12	67.9	185.3
26	a027	136.9	112.5	0.2189	0.00296	17.5131	0.22732	0.5802	0.00585	**2973**	**12**	2963	12	2950	24	0.4	0.8
27	a028-rim	237.3	15.0	0.0920	0.00268	1.8014	0.01732	0.1420	0.00401	1467	32	1046	6	856	23	22.2	71.4
28	a029	185.8	196.8	0.1083	0.00155	4.6741	0.06419	0.3130	0.00315	**1772**	**15**	1763	11	1755	15	0.5	1.0
29	a030	151.2	198.8	0.2035	0.00291	15.5082	0.21311	0.5527	0.00559	**2855**	**13**	2847	13	2837	23	0.4	0.6
30	a031-center	186.8	314.5	0.1015	0.0015	4.0913	0.0585	0.2924	0.00301	**1652**	**16**	1653	12	1654	15	–0.1	–0.1
31	a032	244.9	377.7	0.1020	0.00155	3.9404	0.05804	0.2801	0.00291	**1661**	**16**	1622	12	1592	15	1.9	4.3
32	a033	146.5	214.0	0.1048	0.00158	4.3923	0.06421	0.3040	0.00314	**1711**	**16**	1711	12	1711	16	0.0	0.0
33	a034	129.3	182.4	0.1356	0.00203	7.4450	0.10816	0.3984	0.00412	**2171**	**15**	2166	13	2162	19	0.2	0.4

Table 1. (Contd.)

Ord. no.	Analysis no. in sample	U, ppm	Th, ppm	Measured ratios (corrected for common Pb)						Age, Ma						D1, %	D2, %
				$^{207}Pb/^{206}Pb$	±1σ	$^{207}Pb/^{235}U$	±1σ	$^{206}Pb/^{238}U$	±1σ	$^{206}Pb/^{238}U$	±1σ	$^{207}Pb/^{235}U$	±1σ	$^{207}Pb/^{206}Pb$	±1σ		
34	a035	238.6	264.5	0.2308	0.00493	10.6732	0.10054	0.3354	0.00657	3058	20	2495	9	1865	32	33.8	64.0
35	a036	69.9	66.9	0.0975	0.00211	2.3163	0.02383	0.1723	0.0034	1577	24	1217	7	1025	19	18.7	53.9
36	a037	162.7	138.8	0.0946	0.00152	3.4669	0.05375	0.2660	0.00277	**1519**	**17**	1520	12	1520	14	0.0	–0.1
37	a038	77.1	50.8	0.0626	0.00231	0.9664	0.03459	0.1120	0.0016	694	46	687	18	**684**	**9**	0.4	1.5
38	a039	129.0	92.0	0.2181	0.00507	13.2056	0.12047	0.4392	0.00954	2967	22	2694	9	2347	43	14.8	26.4
39	a040	120.0	53.3	0.0810	0.00146	2.0815	0.03639	0.1865	0.002	1220	21	1143	12	1102	11	3.7	10.7
40	a041	869.8	740.4	0.1284	0.00182	3.0042	0.02086	0.1698	0.00216	2076	14	1409	5	1011	12	39.4	105.3
41	a042	96.2	85.5	0.1264	0.0017	6.5064	0.08413	0.3733	0.00379	**2049**	**14**	2047	11	2045	18	0.1	0.2
42	a043	438.0	620.9	0.1033	0.00153	2.2906	0.01727	0.1608	0.00213	1684	15	1209	5	961	12	25.8	75.2
43	a044	26.5	42.8	0.0917	0.002	3.1214	0.06548	0.2468	0.00296	**1462**	**24**	1438	16	1422	15	1.1	2.8
44	a045	520.2	633.2	0.0524	0.00135	0.3744	0.00931	0.0518	0.0006	303	35	323	7	**326**	**4**	–0.9	–7.1
45	a046	163.8	128.5	0.1076	0.00154	4.6485	0.06377	0.3135	0.0032	**1758**	**15**	1758	11	1758	16	0.0	0.0
46	a047	745.5	671.9	0.0820	0.00111	2.4063	0.03135	0.2129	0.00212	**1245**	**15**	1244	9	1244	11	0.0	0.1
47	a048	135.0	164.2	0.1285	0.00187	6.6934	0.09341	0.3777	0.00387	**2078**	**15**	2072	12	2066	18	0.3	0.6
48	a049	847.2	1029.5	0.1857	0.00335	3.5992	0.02838	0.1405	0.00227	2705	18	1549	6	848	13	82.7	219.0
49	a050	39.1	21.7	0.1920	0.003	13.8811	0.20861	0.5244	0.00567	**2759**	**15**	2742	14	2718	24	0.9	1.5
50	a051	146.6	43.9	0.0557	0.00136	0.5303	0.01254	0.0690	0.00079	442	32	432	8	**430**	**5**	0.5	2.8
51	a052	108.7	100.4	0.0784	0.0011	2.1298	0.02911	0.1969	0.00202	**1158**	**16**	1159	9	1159	11	0.0	–0.1
52	a053	211.9	151.0	0.0793	0.00105	2.2080	0.02852	0.2019	0.00205	**1180**	**15**	1184	9	1185	11	–0.1	–0.4
53	a054	211.1	94.9	0.0793	0.00107	2.2018	0.02898	0.2015	0.00205	**1179**	**15**	1182	9	1183	11	–0.1	–0.3
54	a055	0.2	0.4	0.6562	0.12195	95.0768	18.98061	1.0509	0.20768	4638	159	4635	201	4630	653	0.1	0.2
55	a056	115.3	122.0	0.0787	0.00116	2.1969	0.03162	0.2025	0.00211	**1165**	**17**	1180	10	1189	11	–0.8	–2.0
56	a057-center	110.1	118.7	0.0979	0.00145	3.7485	0.05427	0.2777	0.00292	**1585**	**16**	1582	12	1580	15	0.1	0.3
57	a058-core	832.6	778.0	0.0534	0.00082	0.4003	0.00602	0.0544	0.00056	345	20	342	4	**341**	**3**	0.3	1.2
58	a059	162.3	145.4	0.0595	0.00145	0.6441	0.01523	0.0786	0.00092	584	31	505	9	488	5	3.5	19.7
59	a060	208.6	168.4	0.1285	0.00185	6.7154	0.09453	0.3790	0.00396	**2078**	**14**	2075	12	2072	19	0.1	0.3
60	a061	94.8	206.2	0.0657	0.00111	1.1557	0.01899	0.1276	0.00136	797	20	780	9	**774**	**8**	0.8	3.0
61	a062	78.4	66.1	0.1005	0.0016	4.0460	0.06279	0.2921	0.00316	**1633**	**18**	1643	13	1652	16	–0.5	–1.2
62	a063	557.1	344.1	0.0530	0.00089	0.4028	0.00658	0.0551	0.00058	328	22	344	5	**346**	**4**	–0.6	–5.2
63	a064	272.5	298.7	0.0535	0.00135	0.4287	0.01056	0.0582	0.00068	349	33	362	8	**364**	**4**	–0.5	–4.1
64	a065-core	67.6	95.5	0.0723	0.00143	1.6708	0.03225	0.1676	0.00189	995	23	997	12	**999**	**10**	–0.2	–0.4
65	a066	47.6	42.8	0.0824	0.00147	2.4279	0.04224	0.2138	0.00236	**1254**	**20**	1251	13	1249	13	0.2	0.4
66	a067	52.6	0.3	0.1142	0.00186	5.2809	0.08433	0.3356	0.00366	**1867**	**17**	1866	14	1865	18	0.1	0.1
67	a068	151.5	157.1	0.0948	0.00147	3.4950	0.05319	0.2673	0.00283	**1525**	**17**	1526	12	1527	14	–0.1	–0.1

Table 1. (Contd.)

Ord. no.	Analysis no. in sample	U, ppm	Th, ppm	Measured ratios (corrected for common Pb)						Age, Ma						D1, %	D2, %
				$^{207}Pb/^{206}Pb$	±1σ	$^{207}Pb/^{235}U$	±1σ	$^{206}Pb/^{238}U$	±1σ	$^{206}Pb/^{238}U$	±1σ	$^{207}Pb/^{235}U$	±1σ	$^{207}Pb/^{206}Pb$	±1σ		
68	a069-rim	75.2	116.8	0.0981	0.00202	3.5719	0.07153	0.2640	0.00313	**1589**	**22**	1543	16	1510	16	2.2	5.2
69	a070	159.8	165.1	0.1266	0.00204	6.4095	0.10143	0.3674	0.00395	**2051**	**17**	2034	14	2017	19	0.8	1.7
70	a071	53.4	38.5	0.0788	0.00122	2.1528	0.03247	0.1982	0.00211	**1167**	**18**	1166	10	1165	11	0.1	0.2
71	a072	238.8	385.8	0.1281	0.00182	5.7979	0.08062	0.3282	0.00353	2072	14	1946	12	1830	17	6.3	13.2
72	a073-core	101.3	101.6	0.2137	0.00309	14.8842	0.11417	0.5051	0.00637	2934	14	2808	7	2635	27	6.6	11.3
73	a074	417.6	443.1	0.0534	0.00109	0.4057	0.00808	0.0552	0.00061	344	26	346	6	**346**	**4**	0.0	−0.6
74	a075-rim	171.7	9.6	0.0601	0.00234	0.7521	0.02836	0.0908	0.00133	606	48	569	16	**560**	**8**	1.6	8.2
75	a076	81.1	105.7	0.1009	0.00158	4.0368	0.0617	0.2901	0.00315	**1641**	**17**	1642	12	1642	16	0.0	−0.1
76	a077	60.7	84.0	0.1191	0.00189	5.7722	0.08914	0.3514	0.00387	**1943**	**16**	1942	13	1941	18	0.1	0.1
77	a078	271.3	173.7	0.1117	0.00165	3.5493	0.05095	0.2305	0.00244	1827	15	1538	11	1337	13	15.0	36.6
78	a079	97.5	94.5	0.0710	0.00114	1.5653	0.02437	0.1600	0.00169	956	19	957	10	**957**	**9**	0.0	−0.1
79	a080	456.7	758.9	0.0703	0.00104	1.5210	0.02183	0.1569	0.00162	938	18	939	9	**939**	**9**	0.0	−0.1
80	a081-rim	207.1	143.5	0.0779	0.00126	2.0879	0.03278	0.1944	0.00208	**1144**	**18**	1145	11	1145	11	0.0	−0.1
81	a081-core	261.7	153.4	0.0793	0.00129	1.9868	0.03133	0.1818	0.00194	**1178**	**18**	1111	11	1077	11	3.2	9.4
82	a082	340.9	297.3	0.8268	0.01425	9.8256	0.0735	0.0862	0.00134	4969	14	2419	7	533	8	353.8	832.3
83	a083	46.3	39.8	0.0827	0.00147	2.2917	0.03943	0.2010	0.00221	**1262**	**21**	1210	12	1181	12	2.5	6.9
84	a084-core	133.1	120.6	0.0745	0.00137	1.8039	0.03222	0.1757	0.00194	**1054**	**21**	1047	12	1044	11	0.3	1.0
85	a085	310.8	456.1	0.1114	0.00167	2.6267	0.03813	0.1710	0.0018	1823	16	1308	11	1018	10	28.5	79.1
86	a086	36.6	51.3	0.1881	0.00292	13.6207	0.20623	0.5252	0.00586	**2726**	**15**	2724	14	2721	25	0.1	0.2
87	a087-core	42.5	9.9	0.8035	0.01167	199.1671	2.96973	1.7980	0.02198	4928	12	5381	15	6633	51	−18.9	−25.7
88	a088	196.1	163.4	0.1411	0.00281	5.1118	0.04692	0.2628	0.00474	**2240**	**20**	1838	8	1504	24	22.2	48.9
89	a089	656.9	500.0	0.0530	0.00092	0.3774	0.00634	0.0517	0.00054	328	22	325	5	**325**	**3**	0.0	0.9
90	a090	172.9	196.1	0.1039	0.0016	4.2929	0.06412	0.2998	0.00314	**1694**	**17**	1692	12	1691	16	0.1	0.2
91	a091	3.3	0.3	0.1381	0.01015	3.8314	0.2672	0.2012	0.0066	2204	75	1599	56	1182	35	35.3	86.5
92	a092	115.4	90.7	0.0789	0.00125	2.1729	0.03344	0.1997	0.00212	**1170**	**18**	1172	11	1174	11	−0.2	−0.3
93	a093-core	336.2	266.4	0.0894	0.00128	2.9100	0.0406	0.2360	0.00245	**1413**	**16**	1384	11	1366	13	1.3	3.4
94	a094-core	360.6	250.3	0.0552	0.00103	0.5315	0.00969	0.0699	0.00075	420	24	433	6	**435**	**5**	−0.5	−3.4
95	a095-rim	157.3	52.9	0.0534	0.00161	0.3720	0.01086	0.0505	0.00062	345	39	321	8	<u>**318**</u>	<u>**4**</u>	0.9	8.5
96	a096-core	61.4	74.6	0.0800	0.00191	2.0612	0.04778	0.1869	0.0023	**1197**	**27**	1136	16	1105	12	2.8	8.3
97	a097	170.7	175.5	0.0793	0.00132	2.1685	0.03501	0.1983	0.00212	**1181**	**19**	1171	11	1166	11	0.4	1.3
98	a098	157.7	108.4	0.1008	0.00155	3.9035	0.05854	0.2808	0.00297	**1639**	**16**	1614	12	1595	15	1.2	2.8
99	a099	97.6	76.6	0.1097	0.00171	4.8492	0.07365	0.3205	0.00341	**1795**	**16**	1793	13	1792	17	0.1	0.2
100	a101	1846.6	879.8	0.1494	0.0024	0.9207	0.00751	0.0447	0.00064	**2339**	**16**	663	4	282	4	135.1	729.4
101	a102	18.7	3.2	0.1308	0.00351	5.0741	0.13122	0.2813	0.00421	**2109**	**27**	1832	22	1598	21	14.6	32.0

Table 1. (Contd.)

Ord. no.	Analysis no. in sample	U, ppm	Th, ppm	Measured ratios (corrected for common Pb) $^{207}Pb/^{206}Pb$	±1σ	$^{207}Pb/^{235}U$	±1σ	$^{206}Pb/^{238}U$	±1σ	Age, Ma $^{206}Pb/^{238}U$	±1σ	$^{207}Pb/^{235}U$	±1σ	$^{207}Pb/^{206}Pb$	±1σ	D1, %	D2, %
102	a103	103.1	80.5	0.0881	0.00137	2.8999	0.04437	0.2389	0.00258	**1384**	**17**	1382	12	1381	13	0.1	0.2
103	a105	141.7	39.6	0.1276	0.00187	6.6113	0.09494	0.3758	0.00404	**2065**	**15**	2061	13	2057	19	0.2	0.4
104	a106	1.7	0.5	0.2916	0.01715	4.3899	0.2256	0.1092	0.00373	3426	54	1710	43	668	22	156.0	412.9
105	a107	300.9	87.8	0.1743	0.00331	5.0610	0.04159	0.2106	0.00364	2599	18	1830	7	1232	19	48.5	111.0
106	a108	1201.4	186.8	0.0525	0.00094	0.3656	0.00642	0.0506	0.00055	306	23	316	5	**<u>318</u>**	**<u>3</u>**	–0.6	–3.8
107	a109	256.4	245.5	0.1020	0.00156	4.1312	0.06176	0.2938	0.00313	**1661**	**17**	1660	12	1660	16	0.0	0.1
108	a110	232.7	159.9	0.0799	0.00189	1.9927	0.04576	0.1808	0.00223	1195	26	1113	16	1072	12	3.8	11.5
109	a111	211.8	366.4	0.1029	0.00188	3.2342	0.02891	0.2279	0.00383	1678	19	1465	7	1323	20	10.7	26.8
110	a112-core	316.8	132.8	0.0998	0.00223	1.8317	0.02102	0.1331	0.00266	1620	24	1057	8	806	15	31.1	101.0
111	a113	314.0	117.9	0.0570	0.00098	0.6287	0.01054	0.0800	0.00084	491	23	495	7	**496**	**5**	–0.2	–1.0
112	a114	1336.0	874.9	0.1558	0.00241	2.3059	0.03463	0.1074	0.00112	2410	15	1214	11	657	7	84.8	266.8
113	a115	89.7	58.0	0.0884	0.00158	2.9356	0.05117	0.2408	0.00264	**1391**	**20**	1391	13	1391	14	0.0	0.0
114	a116-core	318.1	610.3	0.1158	0.00249	4.4276	0.04191	0.2773	0.00549	1892	23	1718	8	1578	28	8.9	19.9
115	a117-core	188.5	66.6	0.0965	0.00182	3.4505	0.06328	0.2594	0.00291	**1557**	**21**	1516	14	1487	15	2.0	4.7
116	a118	95.8	52.1	0.0748	0.00137	1.8557	0.03326	0.1799	0.00196	**1063**	**22**	1065	12	1067	11	–0.2	–0.4
117	a119-core	264.6	141.4	0.0746	0.00153	1.8381	0.03666	0.1786	0.00202	**1059**	**24**	1059	13	1059	11	0.0	0.0
118	a120	185.7	133.4	0.1080	0.0019	4.6921	0.08088	0.3150	0.00342	**1767**	**19**	1766	14	1765	17	0.1	0.1
119	a121	1017.1	667.8	0.1190	0.00155	3.6143	0.046	0.2203	0.00225	1941	13	1553	10	1283	12	21.0	51.3
120	a122	403.3	385.3	0.0978	0.00136	3.3825	0.04588	0.2510	0.00261	**1582**	**15**	1500	11	1443	13	4.0	9.6
121	a123	133.0	147.7	0.0804	0.00125	2.2872	0.03463	0.2063	0.00219	**1207**	**17**	1208	11	1209	12	–0.1	–0.2
122	a124	281.1	51.7	0.0689	0.00101	1.4131	0.02018	0.1487	0.00155	896	17	894	8	**894**	**9**	0.0	0.2
123	a125	204.5	176.8	0.0811	0.00136	2.3318	0.03826	0.2085	0.00227	**1225**	**19**	1222	12	1221	12	0.1	0.3
124	a126	97.8	83.9	0.1315	0.00196	7.0267	0.10261	0.3875	0.00415	**2118**	**15**	2115	13	2111	19	0.2	0.3
125	a127-rim	205.6	295.5	0.3355	0.00711	5.5284	0.05471	0.1195	0.00229	3643	19	1905	9	728	13	161.7	400.4
126	a128	42.7	56.8	0.1669	0.00255	11.0183	0.16549	0.4789	0.00522	**2527**	**15**	2525	14	2522	23	0.1	0.2
127	a129-rim	173.6	115.0	0.0711	0.00137	1.5005	0.02824	0.1531	0.00172	961	22	931	11	**918**	**10**	1.4	4.7
128	a130	1729.8	1287.9	0.0647	0.00128	0.2716	0.00245	0.0305	0.00056	763	24	244	2	194	3	25.8	293.3
129	a131	255.8	261.4	0.1502	0.00348	1.4160	0.0156	0.0684	0.00142	2348	22	896	7	426	9	110.3	451.2
130	a132	371.6	239.8	0.0927	0.00149	3.14693	0.04982	0.2463	0.00264	**1481**	**18**	1444	12	1419	14	1.8	4.4

Values taken for the zircon age are highlighted in bold ($^{206}Pb/^{238}U$ and $^{207}Pb/^{206}Pb$ ratios were used in calculations at the age of <1 Ga and ≥1 Ga, respectively). Minimum and maximum ages of detritus zircon grains in the sample are underlined. (D1 and D2) Dating discordance (D1 = 100% × ($^{207}Pb/^{235}U$) age/($^{206}Pb/^{238}U$) age – 1)), (D2 = 100% × ($^{207}Pb/^{206}Pb$) age/($^{206}Pb/^{238}U$) age – 1)). Bar charts and PDC took into account the analyses with the following D value range: –10% <D1, D2 <10% (discarded analyses are marked with a gray background). The correction for common Pb was based on the ComPbCorr software package presented in (Andersen, 2008). Theoretical substantiations for the correction and its formulas are given in (Andersen, 2002). Distortion of the U–Th–Pb isotope system in zircon grains is estimated based on the measured contents of ^{206}Pb, ^{207}Pb, and ^{208}Pb in zircon and the known isotope ratios between Pb isotopes, which are accepted in the software package as $^{206}Pb/^{204}Pb$ = 18.7, $^{207}Pb/^{204}Pb$ = 15.628, and $^{208}Pb/^{204}Pb$ = 38.63.

1846 ppm and from 0.3 to 1287 ppm, and the Th/U value varies from 0.005 to 3.44 (Fig. 7d).

The Th/U ratio is high (>1.0) for more than one-third of the analyzed dZr grains, >1.5 for 13 grains, and >2.0 for four grains. Such high values are often recorded in zircon from the melanocratic (mafic) rocks (Kaczmarek et al., 2008; Linnemann et al., 2011) and/or rocks formed under high-temperature and medium-pressure metamorphism (Wanless et al., 2011).

Analyses of five dZr grains yielded Th/U values <0.1. Such low Th/U values are considered statistically typical of the metamorphogenic zircon crystals. For example, it is shown in (Skublov et al., 2012) that zircon from eclogites is characterized by decreased Th/U values (<0.1), and decreased absolute contents of Th (3 ppm or lower) and U (100 ppm or lower), as well as other features of the REE content. Note that low Th/U values (<0.1) are rare, and they are recorded in zircon from igneous rocks, for example, in very rare ("exotic") rock complexes of ultra-low temperature granitoids (Harrison et al., 2007).

In the remaining dZr grains, Th/U values are recorded within 0.1–1.0 (mainly within 0.5–1.0), which are considered statistically typical for the magmatogenic zircon from the felsic and intermediate igneous rocks (Hoskin and Schaltegger, 2003; Kirkland et al., 2015; Rubatto, 2017).

Thus, about one-third of the studied dZr grains in sandstones from the studied middle Danian fragment of the Novorossiisk–Anapa flysch section was derived primarily from high-silica granitoids and/or their volcanic analogs, as well as plutons and/or their moderate-silica volcanic analogs. For a high proportion of dZr grains from the studied sample, the primary source could be represented by the melanocratic (mafic) rocks. Some dZr grains could be derived from rare ("exotic") rock complexes, such as eclogites, high-temperature metamorphic or ultra-low temperature granitoids.

All age determinations with discordance |D1 & D2| >10% were excluded from consideration. The remaining datings (n = 91) were used to draw bar charts and PDC (Figs. 8a, 8b). The PDC shows the following peaks supported by three or more measurements (Ma): 344 (bright), 901, 1073, 1174 (bright), 1391, 1531, 1655, 1770, and 2071. The maximum age is 2973 ± 12 Ma (a27, D1 = 0.44%, D2 = 0.78%). The minimum is 318 ± 3 Ma (a108, D1 = –0.6%, D2 = –3.8%). The weighted average age of the four youngest dZr grains showed a value of 322 ± 7 Ma (Fig. 7c). There are no obvious regularities between the U–Pb age and Th/U values for these grains from sandstones (sample K21–012) in the studied Danian fragment of the Novorossiisk–Anapa flysch section (Fig. 8c).

DISCUSSION

Currently, we know only two works with the U–Pb dating of dZr from sandstones and sands in pre-Quaternary sequences of the Western Caucasus and West Kuban Trough. All data are summarized in Fig. 8, with the provenance signals designated from **Z1** to **Z5**.

Provenance signals **Z1** and **Z2**. Bar charts of U–Pb (SHRIMP) values of the dZr age in Oligocene sandstones at vicinities of the Mamayka Settlement (**Z1**, Matsesta Formation) and the Shilovka Settlement (**Z2**, Khosta Formation) on the southern slope of the Western Caucasus are presented in (Mityukov et al., 2011).

Provenance signals **Z3**–**Z5**. Analyses of the mineralogy of Cenozoic sandstones in the Northern Black Sea region—Taman Peninsula, Cis-Caucasus (Indolo-Kuban trough) and various regions of the Western and Central Caucasus—are presented in (Vincent et al., 2013). These results did not reveal signs of erosion of the Caucasus in the Early Neogene. For five of these samples, the paper also provides information about the U–Pb ages of dZr grains obtained using the SHRIMP-RG technology. In particular, one sample (**Z3**, WC99/3, n = 70) characterizes sandstones included in the Oligocene (Rupelian) flyschoid section exposed on the northern outskirts of the Novaya Shilovka Settlement about 7.5 km NW from the Adler airport (southern slope of the Western Caucasus). The second sample (**Z4**, WC139/1, n = 70) characterizes the Miocene(?)–Lower Pliocene (Pliocene/Pleistocene boundary horizons, i.e., between Messinian and Zanclian) alluvial sands recovered in the Tsymbal quarry in the northern Sennaya Settlement located at the apex of the Taman Bay (southern slope of the Western Caucasus). The third sample (**Z5**, ILN-13, n = 68) characterizes sublitharenite sandstones in the middle part of the section (Chattian and Aquitanian stages) of the Maikop Group drilled (depth 700–706 m) on the right bank of the Kuban River about 25 km north of Temizhbek station.

Unfortunately, the above-mentioned materials do not fit modern requirements and standards for such kind of data.

Firstly, the dZr age sets discussed in these papers are not statistically representative, since they include only 50 datings in (Mityukov et al., 2011) and only 70 or less datings in (Vincent et al., 2013), and even less if we take into account the selection based on the degree of discordance. This number is significantly less than the value needed for the statistically reliable and representative data, according to recommendations in (Andersen, 2005; Vermeesch, 2004, 2012).

Secondly, the presented geochronological data are methodically imperfect. In the primary numerical tables presented in (Vincent et al., 2013) for the datings calculated from the $^{206}Pb/^{238}U$ ratio, there is no information about the measured $^{207}Pb/^{235}U$ and

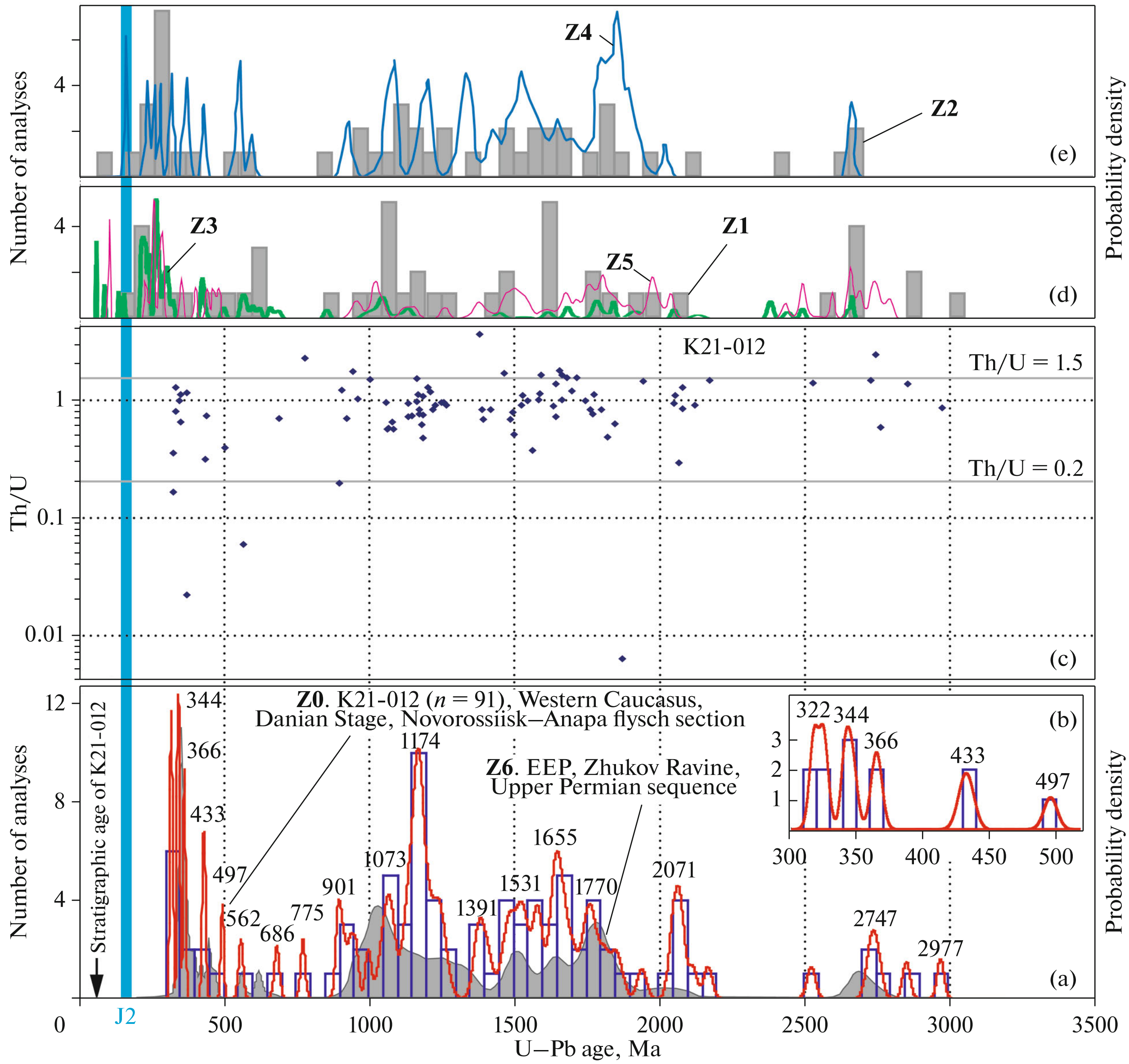

Fig. 8. Comparison of the obtained data on the U–Th–Pb isotopic system of detritus zircon grains from sandstones in sample K21-012 (taken from the middle Danian fragment of the Novorossiisk–Anapa flysch section) versus similar data on sandstones and sands from pre-Quaternary sequences of the Western Caucasus and other regions. Blue band (J2) marks the Middle Jurassic magmatism widely manifested in the Crimea and Western Caucasus. (a) Bar chart and probability density curve (PDC) of dZr ages in sample K21-012 (provenance signal **Z0**) and PDC of similar data on the Late Permian–Early Triassic sequence in the Moscow syneclise, Zhukov Ravine reference section (provenance signal **Z6**), according to (Chistyakova et al., 2020); (b) closeup of PDC (a); (b) Th/U vs. U–Pb age diagram, sample K21-012; (d, e) PDC or bar charts of U–Pb ages of dZr from sandstones in the Cenozoic sequences in the Western Caucasus and West Kuban trough: **Z1 (bar chart)** sandstones of the Oligocene Matsesta Formation, Bolshoi Sochi, Shilovka Settlement, Western Caucasus, southern slope. Sample Ep-1/1 (n = 50), adopted from (Mityukov et al., 2011); **Z2 (bar chart)** sandstones of the Oligocene Khosta Formation, Bolshoi Sochi, Mamaika Settlement, Western Caucasus, southern slope; sample Ma-2/1 (n = 50), adopted from (Mityukov et al., 2011); **Z3 (PDC) Western Caucasus**, southern slope, Lower Oligocene (lower Maikopian) sandstones; sample WC-99/3 (n = 70), adopted from (Vincent et al., 2013); **Z4 (PDC)** sandstones at boundary levels of the section between the Upper Miocene and Lower Pliocene (Cimmerian), Taman Peninsula, periclinal subsidence of the western segment of the Greater Caucasus; sample WC-139/1) (n = 70), adopted from (Vincent et al., 2013); **Z5 (PDC)** sandstones in the Upper Oligocene–Lower Miocene fragment of the middle part of the Maikop Group section, Indolo–Kuban trough; sample ILN#13_700 was taken from the borehole core recovered from a depth of 700–706 m (n = 68), adopted from (Vincent et al., 2013).

$^{207}Pb/^{206}Pb$ ratios and the ages obtained from them. This fact does not allow us to calculate the discordance index of single isotope analyses and carry out the necessary selection of analytical results according to their quality. It is possible that, among other things, the PDC curves in (Vincent et al., 2013) are based on significantly discordant age estimates that should be excluded from consideration.

In addition, there is no information about reproducibility of the datings of zircon standards, confirming the stability of equipment during the measurements, the reliability of isotope datings of the studied dZr, and so on.

All these reasons compel us to qualify the available data only as preliminary materials that need further confirmation. Neither individual peak PDC values nor, the more so, the ages of individual dZr grains can be interpreted meaningfully. Only the generalized characteristics of the provenance signal of the studied sequences, such as approximate time intervals of large dZr groups, approximate quantitative ratios between these groups, and other parameters can be used for the comparison with similar data on other sequences.

Comparison of new data on the U–Pb ages of dZr from sandstones in the Danian section of the Novorossiisk–Anapa flysch (**Z0**, sample K21-012) with the previously obtained similar pilot data on the Matsesta (**Z1**) and Khosta (**Z2**) formations, as well as sandstones in the flyschoid section near the Novaya Shilovka Settlement (**Z3**) (all sites are located on the southern slope of the Western Caucasus), Taman Peninsula (**Z4**), and Indolo–Kuban Trough (**Z5**) (Fig. 8) revelaed a general similarity in the age distribution. All provenance signals include the scattered Archean datings and lack the Early Paleoproterozoic datings. The Middle–Late Paleoproterozoic, Mesoproterozoic, and Early Neoproterozoic are represented slightly more quantitatively than the Archean, but also without the formation of any compact coeval dZr groups. The Middle Neoproterozoic is virtually absent, and the Late Neoproterozoic and Early Paleozoic are represented by single grains.

In the younger portion of the age spectrum, provenance signals **Z0**–**Z5** are marked by visible differences. Signal **Z0** includes compact group of six Carboniferous ages, but grains younger than ~320 Ma are absent. Signals **Z1**–**Z5** include a group of Permian–Triassic (300–200 Ma) zircon grains and single younger grains. We note this fact but do not interpret it in any way, since the data on **Z1**–**Z5** are hardly reliable (see comments above).

The age of the studied Novorossiisk–Anapa flysch sequence (**Z0**, sample K21-012) is limited to an interval of 63.9–65.3 Ma, and the youngest dZr dating of sandstones in this sequence is about 320 Ma. Thus, the time gap is more than 250 Ma! During this interval, the Crimean–Caucasian Basin underwent tectonic events accompanied by magmatic activity and the formation of zircon-bearing crystalline complexes, such as the widespread Middle Jurassic magmatism in the Caucasus and Crimea. For several magmatites in the Crimea and Western/Central Caucasus, the Jurassic age has been confirmed reliably by modern high-precision geochronological datings:

(1) rocks of the Jurassic basalt–andesite–dacite association in the Karachay volcanic region (Central Caucasus) with an age of ~185 Ma, based on the Ar–Ar dating of mineral fractions of biotites and feldspars (Gurbanov et al., 2011);

(2) rocks of the bimodal magmatic association in the Khulam volcanoplutonic complex with an age of 167 ± 4.4 Ma, common in the Kabardino–Balkaria region (central part of the Northern Caucasus), based on the U–Pb and K–Ar datings (Kaigorodova, 2022; Kaigorodova and Lebedev, 2022);

(3) basalt flows (subvolcanic bodies) common on the outskirts of the Maloe Pseushko Settlement (Western Caucasus), with the U–Pb SHRIMP age of the accessory zircon estimated at 169 ± 1.5 Ma (Gerasimov et al., 2022);

(4) rhyodacite bodies (about 170 Ma) near the top of Mt. Indyuk (Western Caucasus) (our unpublished data);

(5) volcanites of Karadag (eastern Crimean Mountains), with the Ar–Ar age of 172.8 ± 4.5 Ma (Popov et al., 2019);

(6) dolerites of the Pervomaisk stock (174.2 ± 1.2 Ma and gabbro-dolerites of the Dzhidair pluton (169.7 ± 1.5 Ma) in the vicinity of the Trudolyubovka Settlement (central Crimean Mountains), U–Pb SHRIMP dating data (Morozova et al., 2017); and

(7) plagiorhyolites of the Monakh Clift in the Cape Fiolent area (western Crimean Mountains) with an age of 168.3 ± 1.3 Ma (Kuznetsov et al., 2022).

Note that the above-listed magmatite bodies (3) and (4) are located very near (just about 20–30 km away) from the K21-12 sampling site. However, zircon with the Jurassic age was not recorded in sandstones from this sample (Figs. 8a, 8b); i.e., there are no signs of the erosion of Jurassic magmatic complexes in the Crimea or Western Caucasus and the transport of their erosion products into the studied Novorossiisk–Anapa flysch sequence.

Comparison of the set of dZr ages from sample K21-012 with similar data (**Z6**) on sandstones of the red-colored Upper Permian sequence in the Moscow syneclise in the Zhukov Ravine reference section (Chistyakova et al., 2020) revealed their amazing similarity (Fig. 8a). In addition, frequency peaks in the age sets of dZr from modern alluvial sands in lower reaches of the Volga (Allen et al., 2006, Koltringer et al., 2022) and Don (Koltringer et al., 2022) rivers and from sandstones of sample K21-012 are similar. All this clearly indicates that the detrital material com-

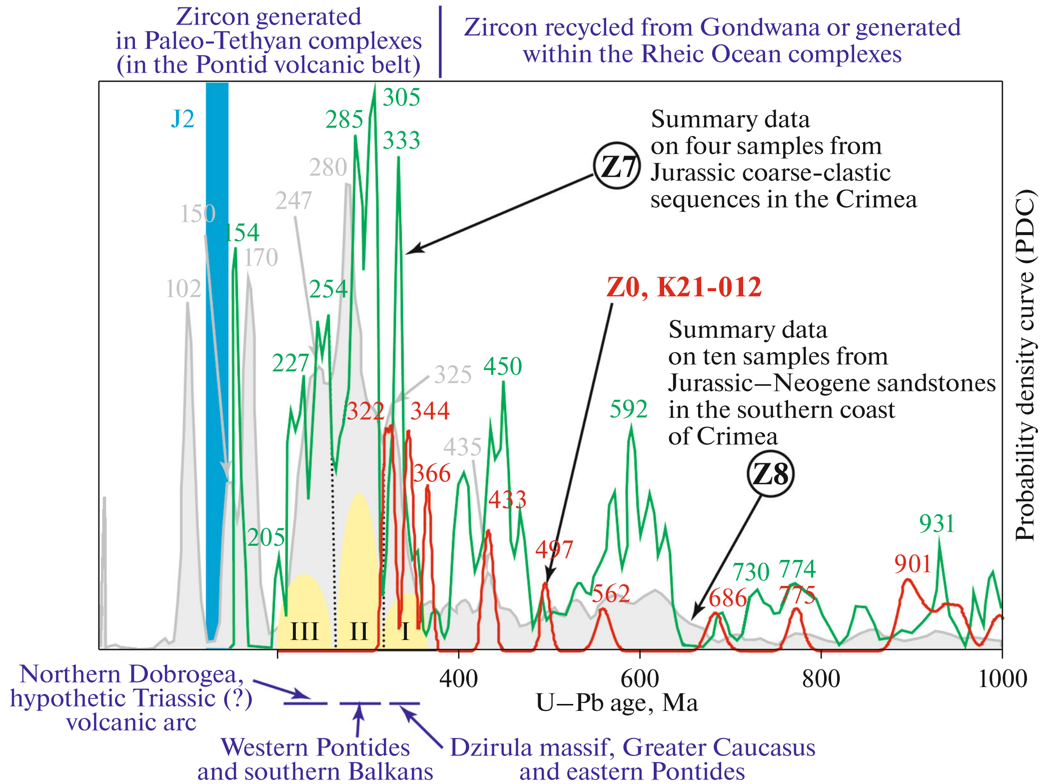

Fig. 9. Comparison of probability density curves (PDC) of the U–Pb age of detrital zircon grains from sample K21-012 with similar data for Crimea in the age range of <1 Ga. In circles: (**Z7**) integral PDC value summing up the results of U–Pb dating of detritus zircon grains from the Middle and Upper Jurassic coarse-clastic sequences in the Crimean Mountains (four samples in different geographical locations, $n = 269$, according to (Romanyuk et al., 2020); (**Z8**) integral PDC summing up the data on nine samples from the Middle Jurassic–Neogene sandstones in the Crimean Mountains, according to (Nikishin et al., 2015a), $n = 602$). (n) Number of analyses used for the PDC construction. Yellow ovals mark three stages of magmatic activity manifested in the Scythian–Pontid volcanic belt: 360–315 Ma, 315–270 Ma, and 270–200 Ma. The blue band (J2) marks the Middle Jurassic magmatism widely manifested in the Crimean Mountains, Western and Central Caucasus. Information about possible primary sources of different-age zircons is given in the lilac font.

posing the Novorossiisk–Anapa flysch was transported from the EEP.

The results of the dZr study complement the results of the analysis of seismostratigraphic data, clearly indicating that the detrital material was transported in the Paleocene into the northern part of the Crimean–Caucasian Basin (currently identified as the West Kuban trough) from the EEP side located in north. The dZr results suggest that the southern part of the Crimean–Caucasian Basin (currently identified as the Tuapse trough) also received detrital material from the EEP, and there are no signs of erosion of the Caucasian rock complexes hosting the Jurassic magmatites. The bulk of the material was supplied to the basin by the recycled Permian–Triassic and younger EEP sequences. According to our opinion, the latter sequences were formed mainly due to the accumulation of recycled destruction products of crystalline complexes and ancient sedimentary sequences involved in the Late Paleozoic Paleo-Uralian orogen orogen.

Comparison of new data on the U–Pb ages of dZr in the Novorossiisk–Anapa flysch (sample K21-012) with the available similar data on Mesozoic–Cenozoic sequences of the Crimean Mountains (CM) is shown in Fig. 9. Middle Jurassic magmatites are widespread in the CM (see paragraphs 5–7 in the list presented at the beginning of the section). However, no Middle Jurassic dZr grains were detected in the Jurassic coarse-clastic sequences of CM (provenance signal **Z7**). The contribution of a local source with the Late Jurassic age (~154 Ma) was only recorded in one of the four studied sequences (Upper Demerdzhi Formation, southern Demerdzhi Mountain (Kuznetsov et al., 2019; Rudko et al., 2018, 2019). Jurassic magmatic complexes in the eastern and/or central part of the Caucasus were exposed and eroded in the Late Mesozoic and/or Early Cenozoic, and their erosion products were transported to sedimentary sequences in the eastern and central Cis-Caucasia/Trans-Caucasia. This fact is suggested by the presence of numerous Jurassic dZr grains in Bajocian sandstones in the eastern (Allen et al., 2006) and western (Cowgill et al.,

2016) parts of the Greater Caucasus. It is noteworthy that a significant number of Middle Jurassic dZr grains were recorded reliably in the younger CM sequences, according to the summary data on Jurassic–Neogene sandstones on the southern coast of Crimea (Nikishin et al., 2015a) (provenance signal **Z8**), probably, suggesting that the Jurassic magmatite-hosting sequences, exposed now in the Caucasus and CM, were exhumed periodically at different times. In the Western Caucasus and CM, this process took place later than in the Central and Eastern Caucasus.

It is also noteworthy that the Permian–Triassic zircons, which are absent in sandstones from the middle Danian fragment of the Novorossiisk–Anapa flysch section (**Z0**), have been recorded reliably in Jurassic coarse-clastic sequences in CM (**Z7**, Fig. 9). At the same time, analysis of the possible provenances for clastic rocks in these sequences has shown that a significant contribution to sedimentation flows feeding these sequences was provided by the erosion products of crystalline complexes in the Peri-Gondwanan terranes and/or the Rheic Ocean (Kuznetsov and Romanyuk, 2021; Romanyuk et al., 2020).

Available results of the U–Pb dating of dZr from detrital sequences from various stratigraphic levels and geographical locations of the CM and the Caucasus record significant differences in the provenances for the western, central, and eastern parts of the Crimean–Caucasian Basin, as well as a change in the position of detrital material sources during the evolution of this basin. However, a much larger amount of data is needed to determine accurately the time boundaries of critical changes in the sedimentation flow directions, changes in provenances, and segmentation of the Crimean–Caucasian Basin at various stages of the BSBAC region evolution, and detailed paleogeographic reconstructions of this region.

CONCLUSIONS

The first results of the U–Th–Pb isotope dating of dZr from the Middle Danian sandstones in the Cretaceous–Eocene Novorossiisk–Anapa flysch, widely developed in the northern and central parts of the Sochi synclinorium located on the southern slope of the Western Caucasus, are presented. Sample K21-012 was taken in a coastal rock outcrop on the Kiselev Clift located between Tuapse and Agoi Settlement. The nannoplankton assemblage from light gray calcareous silty mudstones in the upper element of the same turbidite rhythm (sample K21-012 was taken from sandstones at its base) has reliably constrained the age of the sampled Novorossiisk–Anapa flysch fragment to an interval of 63.9–65.3 Ma. The U–Th–Pb isotope system was studied for 130 dZr grains. Age estimates for ~35% of grains are characterized by strong discordance, indicating the thermal and/or metasomatic impact (possibly repeated) on the analyzed zircon grains. The bar chart and PDC were plotted based on 91 provisional datings. The maximum age is 2973 ± 12 Ma, the minimum is 318 ± 3 Ma, and the weighted average age of four youngest grains is ~322 ± 7 Ma. The provenance signal includes scattered Archean datings and lack Early Paleoproterozoic values. The Middle and Late Paleoproterozoic, as well as Mesoproterozoic and Early Neoproterozoic are represented by a slightly greater number of datings than the Archean, but also without any compact coeval dZr groups. The Middle Neoproterozoic is virtually absent, whereas the Late Neoproterozoic and Early Paleozoic are represented by single grains. Only six Carboniferous datings make up a compact group manifested with a bright peak (~344 Ma) on the PDC.

Based on the U and Th contents, the main primary source of zircon in the middle Danian sandstones of the Novorossiisk–Anapa flysch was represented, most likely, by the high- and moderate-silica granitoids and/or their volcanic analogs. The melanocratic (mafic) rocks could make a fairly high contribution to the primary sources of zircon. Some dZr grains could be delivered from rare ("exotic") rock complexes, such as eclogites, high-temperature metamorphites, or ultra-low temperature granitoids. There are no obvious regularities or correlations of the U–Pb age of dZr grains in the middle Danian sandstones from the Novorossiisk–Anapa flysch with the Th/U values for these grains.

Comparison of the obtained dZr age sets from sample K21-012 (**Z0**) with the available similar data on Paleogene–Neogene and Early Quaternary (Early Pleistocene) detrital rocks in other regions of the Western Caucasus and Western Cis-Caucasus (**Z1**–**Z5**) showed a general similarity of provenance signals in the Precambrian portion of the dZr age spectrum.

The time gap between the studied middle Danian fragment of the Novorossiisk–Anapa flysch section (**Z0**) and the youngest datings of dZr grains from sandstones of this section is about 250 Ma. During this period (from ~64 to ~322 Ma), Jurassic magmatism was widely manifested in the Crimean–Caucasian Basin and its framing. Some magmatic bodies, whose Jurassic age is confirmed by modern high-precision geochronological dating, are located just 20–30 km away from the K21-012 sampling site. However, Jurassic dZr was not recorded in the sample; i.e., no signs of the erosion of Jurassic magmatic complexes and the input of their erosion products have been recorded in the studied fragment of the Novorossiisk–Anapa flysch.

Comparison of the age set of dZr grains from sample K21-012 with similar data on sandstones in the red-colored Upper Permian sequences of the Moscow syneclise in the Zhukov Ravine reference section (**Z6**) has shown their amazing similarity. Several bright peaks on the PDC of the dZr age sets from the modern alluvial sands in deltas of the Volga and Don rivers (Allen et al., 2006; Koltringer et al., 2022) draining vast areas of the EEP actually repeat the PDC peaks for sample K21-012. All this indicates that the detrital material composing the middle Danian fragment of the Novorossiisk–Anapa flysch section was transported from the EEP.

Pioneer results of the study of dZr grains from sandstones of the middle Danian fragment of the Novorossisk–Anapa flysch section reported in this paper complement the results of the analysis of seismostratigraphic materials related to the West Kuban trough. These data indicate clearly that the detrital material was transported in the Paleocene to the northern Crimean–Caucasian Basin (currently identified as the West Kuban trough) and further southward to those parts of the Crimean–Caucasian Basin, whose relics compose now the Sochi synclinorium, from the north. There are no signs of the erosion of Jurassic magmatite-hosting rocks of the Greater Caucasus. We believe that the detrital material in the more southern part of the Crimean–Caucasian Basin (identified now as the Tuapse trough) was also transported from the EEP.

The bulk of the material was delivered to the basin by the recycled Permian–Triassic and younger EEP sequences, which could be formed mainly due to the accumulation of recycled erosion products of crystalline complexes and ancient sedimentary sequences involved in the Paleo-Uralian Late Paleozoic orogen.

The accumulated results of the U–Th–Pb isotope dating of dZr grains from detrital rocks of various stratigraphic levels and geographical locations within the BSBAC region suggest significant differences in the provenances for the western, central, and eastern parts of the Crimean–Caucasian Basin, as well as their change during the basin evolution. However, a much larger amount of data is needed to constrain accurately time boundaries of the critical changes in sedimentation conditions, sedimentation flow direction, provenances, and segmentation of the Crimean–Caucasian Basin in different time periods and to accomplish detailed reconstructions of paleogeographic conditions.

FUNDING

This work was accomplished in accordance with research plans, project RNF-23-27-00409 (T.V. Romanyuk, supervisor).

CONFLICT OF INTEREST

The authors of this work declare that they have no conflicts of interest.

REFERENCES

Afanasenkov, A.P., Nikishin, A.M., and Obukhov, A.N., *Geological structure and hydrocarbon potential of the eastern Black Sea region*, Moscow: Nauchn. Mir, 2007.

Agnini, C., Fornaciari, E., Raffi, I., Catanzariti, R., Palike, H., Backman, J., and Rio, D., Biozonation and biochronology of Paleogene calcareous nannofossils from low and middle latitudes, *Newslett. Stratigr.*, 2014, vol. 47, no. 2, pp. 131–181.
https://doi.org/10.1127/0078-0421/2014/0042

Aleksandrova, G.N., Erofeeva, K.G., Kuznetsov, N.B., Romanyuk, T.V., Sheshukov, V.S., Dubenskii, A.S., Lyapunov, S.M., Yakovleva, A.I., and Pan'kov, V.N., The First Results of U–Pb Dating of Detrital Zircons from the Oligocene of the Southeastern Part of the Voronezh Anteclise and Their Importance for Paleogeography, *Dokl. Earth Sci.*, 2020, vol. 494, no. 1, pp. 675–679.
https://doi.org/10.31857/S2686739720090042

Allen, M.B., Morton, A.C., Fanning, C.M., Ismail-Zadeh, A.J., and Kroonenberg, S.B., Zircon age constraints on sediment provenance in the Caspian region, *J. Geol. Soc. London*, 2006, vol. 163, pp. 647–655.

Almendinger, O.A., Mityukov, A.V., Myasoedov, N.K., and Nikishin A.M., *Dokl. Earth Sci.*, 2011, vol. 439, no. 1, pp. 899–901.

Andersen, T., Correction of common lead in U–Pb analyses that do not report ^{204}Pb, *Chem. Geol.*, 2002, vol. 192, pp. 59–79.

Andersen, T., Detrital zircons as tracers of sedimentary provenance: limiting conditions from statistics and numerical simulation, *Chem. Geol.*, 2005, vol. 216, pp. 249–270.

Andersen, T., ComPbCorr—Software for common lead correction of U–Th–Pb analyses that do not report ^{204}Pb in LA-ICP-S in the Earth Sciences: Principles and aplications, Sylvester, P.J., Ed., *Miner. Ass. Canada, Short Course Ser.*, 2008, vol. 40, pp. 312–314.

Baskakova, G.V., Vasil'eva, N.A., Nikishin, A.M., Doronina, M.S., and Ikhsanov, B.I., Identification of the main tectonic events by using 2D–3D seismic data in the eastern Black Sea, *Mosc. Univ. Geol. Bull.,* 2022, no. 5, pp. 466–478.

Bol'shoi Kavkaz v al'piiskuyu epokhu (The Greater Caucasus during the Alpine Epoch), Leonov, Yu. G., Ed., Moscow: GEOS, 2007.

Bouma, A.H., *Sedimentology of Some Flysch Deposits*, Amsterdam: Elsevier, 1962.

Chistyakova, A.V., Veselovskii, R.V., Semenova, D.V., Kovach, V.P., Adamskaya, E.V., and Fetisova, A.M., Stratigraphic correlation of Permian–Triassic red beds, Moscow Basin, East European Platform: First detrital zircon U–Pb dating results, *Dokl. Earth Sci.*, 2020, vol. 492, no. 1, pp. 306–310.

Cowgill, E., Forte, A.M., Niemi, N., et al., Relict basin closure and crustal shortening budgets during continental collision: An example from Caucasus sediment provenance, *Tectonics*, 2016, vol. 35, pp. 2918–2947.
https://doi.org/10.1002/2016TC004295

Elhlou, S., Belousova, E.A., Griffin, W.L., Pearson, N.J., and O'Reily, S.Y., Trace element and isotopic composition of GJ-red zircon standard by laser ablation, *Geochim. Cosmochim. Acta*, 2006, vol. 70, no. 18, p. A158.

Geologiya SSSR (Geology of the Soviet Uniomn, Andrushchuk, V.L, Dubinskii, A.Ya, and Khain, V. E., Eds., Moscow: Nedra, 1968, vol. 9 (North Caucasus).

Gerasimov, V.Yu., Ul'yanov, A.A., Snezhko, V.A., Mozar, D., Lavrishchev, V.A., Gazeev, V.M., and Gurbanov, A.G., Zircon isotope dating of Jurassic basalts from the Goitkh volcanic region of the Western Caucasus, *Mosc. Univ. Geol. Bull.*, 2022, no. 2, pp. 192–197.

Griffin, W.L., Powell, W.J., Pearson, N.J., and Reilly, S.Y., GLITTER: data reduction software for laser ablation ICP-MS, in *Laser Ablation ICP-MS in the Earth Sciences: Current Practices and Outstanding Issues*, Sylvester, P.J., Ed., Miner. Ass. Can. Short Course, 2008, vol. 40, pp. 308–311.

Gurbanov, A.G., Gazeev, V.M., Leksin, A.Yu., and Khess, Yu.S., The Lower Jurassic island-arc basal–andesite–dacite magmatism in the Central Caucasus (Karachaevo volcanic region): Petrological-geochemical and isotopic features and genesis, *Vestn. Vladikavkaz. Nauchn. Tsentra*, 2011, vol. 11, no. 2, pp. 15–32.

Harrison, T.M., Watson, E.B., and Aikman, A.B., Temperature spectra of zircon crystallization in plutonic rocks, *Geology*, 2007, vol. 35(7), pp. 635–638. https://doi.org/10.1130/G23505A.1

Hoskin, P.W. and Schaltegger, U., The composition of zircon and igneous and metamorphic petrogenesis, *Rev. Miner. Geochem.*, 2003, vol. 53(1), pp. 27–62.

Horstwood, M.S.A., Kosler, J., Gehrels, G., Jackson, S.E., McLean, N.M., Paton, Ch., Pearson, N.J., Sircombe, K., Sylvester, P., Vermeesch, P., Bowring, J.F., Condon, D.J., and Schoene, B., Community–derived standards for LA-ICP-MS U–(TH–)Pb geochronology – uncertainty propagation, age interpretation and data reporting, *Geostand. Geoanal Res.*, 2016, vol. 40, no. 1, pp. 311–332.

Jackson, S.E., Pearson, N.J., Griffin, W.L., and Belousova, E.A., The application of laser ablation-inductively coupled plasma-mass spectrometry to in situ U–Pb zircon geochronology, *Chem. Geol.*, 2004, vol. 211, pp. 47–69.

Kaczmarek, M.A., Müntener, O., and Rubatto, D., Trace element chemistry and U–Pb dating of zircons from oceanic gabbros and their relationship with whole rock composition (Lanzo, Italian Alps), *Contrib. Mineral. Petrol.*, 2008, vol. 155(3), pp. 295–312. https://doi.org/10.1007/s00410-007-0243-3

Kaigorodova, E.N. Geological features of the Raduzhnoe gold–sulfide deposit (Greater Caucasus and its geological setting), *Extended Abstract, PhD (Geol.–Miner.) Dissertation*, Moscow: IGEM RAN, 2022.

Kaigorodova, E.N. and Lebedev V.A. Age, petrological-geochemical characteristics, and origin of igneous rocks of the Middle Jurassic igneous rocks in the Khulam volcano-plutonic complex (North Caucasus), *Vulkanol. Seismol.*, 2022, no. 2, pp. 38–65. https://doi.org/10.31857/S0203030622020031

Kirkland, C.L., Smithies, R.H., Taylor, R.J.M., Evans, N., and McDonald, B., Zircon Th/U ratios in magmatic environs, *Lithos*, 2015, vol. 212–215, pp. 397–414.

Koltringer, C., Stevens, T., Lindner, M., Baykaa, Y., Ghafarpour, A., Khormali, F., Taratunina, N., and Kurbanov, R., Quaternary sediment sources and loess transport pathways in the Black Sea–Caspian Sea region identified by detrital zircon U–Pb geochronology, *Global Planet. Change*, 2022, vol. 209, p. 103736. https://doi.org/10.1016/j.gloplacha.2022.103736

Korsakov, S.G., Semenukha, I.N., Gorbova, S.M., Zarubin, V.V., Sokolov, V.V., Tuzikov, G.R., Chernykh, V.I., Tereshchenko, L.A., and Andreev, V.M., *Gosudarstvennaya geologicheskaya karta Rossiiskoi Federatsii masshtaba 1 : 200000* (State Gological Map of the Russian Federation), St. Petersburg: Izd-vo Kartfabriki VSEGEI, 2002, Ser. Caucasus, Sheet K-37-XXXIV (Tuapse), Explanatory Note.

Korsakov, S.G., Gorbova, S.M., Kamenev, S.A., Semenukha, I.N., Chernykh, V.I., Sokolov, V.V., Tuzikov, G.R., Saakov, V.G., Prokuronov, P.V., Andreev, V.M., Shel'ting, S.K., Romanova, G.E., Gross, E.G., and Sivukha, N.M., *Gosudarstvennaya geologicheskaya karta Rossiiskoi Federatsii masshtaba 1 : 200000* (State Geological Map of the Russian Federation. Scale 1 : 200000, St. Petersburg, 2021, Ser. Caucasus, Sheet L-37-XXXIV (Gelendzhik), Explanatory Note.

Kuznetsov, N.B. and Romanyuk, T.V., Peri-Gondwanan blocks in the structure of the southern and southeastern framing of the East European Platform, *Geotectonics*, 2021, no. 4, pp. 439–472.

Kuznetsov, N.B., Belousova, E.A., Griffin, W.L., O'Reilly, S.Y., Romanyuk, T.V., and Rud'ko, S.V., Pre-Mesozoic Crimea as a continuation of the Dobrogea platform: Insights from detrital zircons in Upper Jurassic conglomerates, Mountainous Crimea, *Int. J. Earth Sci.*, 2019, vol. 108, no. 7, pp. 2407–2428. https://doi.org/10.1007/s00531-019-01770-2

Kuznetsov, N.B., Romanyuk, T.V., Strashko, A.V., and Novikova, A.S., The ophiolite association on Cape (western Crimean Mountains)—upper age limite based on results of the U–Pb isotope dating of plagiorhyolites (Monakh Clift), *Zap. Gorn. Inst.*, 2022, no. 4, pp. 3–15.

Linnemann, U., Ouzegane, K., Drareni, A., Hofmann, M., Becker, S., Gärtner, A., and Sagawe, A., Sands of West Gondwana: an archive of secular magmatism and plate interactions – a case study from the Cambro-Ordovician section of the Tassili Ouan Ahaggar (Algerian Sahara) using U–Pb-LA-ICP-MS detrital zircon ages, *Lithos*, 2011, vol. 123(1–4), pp. 188–203. https://doi.org/1016/j.lithos.2011.01.010

Ludwig, K.R., *User's Manual for Isoplot 3.75. A Geochronological Toolkit for Microsoft Excel, Berkeley Geochron. Center. Spec. Publ.*, 2012, no. 5.

Marinin, A.V. and Rastsvetaev, L.M., Structural paragenesis in the northwestern Caucasus, in *Problemy tektonofiziki* (Problems in Tectonophysics), Moscow: IFZ RAN, 2008, pp. 191–224 (Collection of Works).

Marinin, A.V., Stupin, S.I., and Kopaevich, L.F., The structure and stratigraphic position of the Agoi Olistostrome, Northwest Caucasus, *Mosc. Univ. Geol. Bull.*, 2017, no. 5, pp. 405–415.

Martini, E., Standard Tertiary and Quaternary calcareous nannoplankton zonation, Frinacci, A., Ed., *Proc. 2nd Plankt. Conf. Plankt. Microfossils*, Roma: Tecnoscienza, 1971, vol. 2, pp. 739–785.

Mityukov, A.V., Al'mendinger, O.A., Myasoedov, N.K., Nikishin, A.M., and Gaiduk, V.V., The sedimentation model of the Tuapse Trough (Black Sea), *Dokl. Earth Sci.,* 2011, vol. 440, no. 3, pp. 1245–1248.

Morozova, E.B., Sergeev, S.A., and Savel'ev, A.D., Cretaceous and Jurassic intrusions in the Crimean Mountains: Fist data on the U–Pb (SIMS SHRIMP) dating, *Dokl. Earth Sci.*, 2017, vol. 474, no. 1, pp. 530–534.

Nikishin, A.M., Ershov, A.V., and Nikishin, V.A., Geological history of Western Caucasus and adjacent foredeeps based on analysis of the regional balanced section, *Dokl. Earth Sci.*, 2010, vol. 430, no. 4, pp. 155–157.

Nikishin, A.M., Wannier, M., Alekseev, A.S., Almendinger, O.A., Fokin, P.A., Gabdullin, R.R., Khudoley, A.K., Kopaevich, L.F., Mityukov, A.V., Petrov, E.I., and Rubtsova, E.V., Mesozoic to recent geological history of southern Crimea and the eastern Black Sea region, Sosson, M., Stephenson, R.A., and Adamia, S.A., Eds., *Tectonic Evolution of the Eastern Black Sea and Caucasus, Geol. Soc. London. Spec. Publ.*, 2015a.
https://doi.org/10.1144/SP428.1

Nikishin, A.M., Okay, A., Tüysüz, O., Demirer, A., Wannier, M., Amelin, N., and Petrov, E., The Black Sea Basins structure and history: new model based on new deep penetration regional seismic data. Part 1. Basins structure, *Mar. Petrol. Geol.*, 2015b, vol. 59, pp. 638–655.
https://doi.org/10.1016/j.marpetgeo.2014.08.017

Nikishin, A.M., Okay, A., Tüysüz, O., Demirer, A., Wannier, M., Amelin, N., and Petrov, E., The Black Sea Basins structure and history: new model based on new deep penetration regional seismic data. Part 2. Tectonic history and paleogeography, *Mar. Petrol. Geol.*, 2015c, vol. 59, pp. 656–670.
https://doi.org/10.1016/j.marpetgeo.2014.08.018

Nikishin, A.M., Romanyuk, T.V., Moskovskii, D.V., Kuznetsov, N.B., Kolesnikova, A.A., Dubenskii, A.S., Sheshukov, V.S., and Lyapunov, S.M., Upper Triassic sequences in the Crimean Mountains: First results of the U–Pb dating of detrital zircons, *Mosc. Univ. Geol. Bull.*. 2020, no. 2, pp. 18–33.

Okay, A.I. and Nikishin, A.M., Tectonic evolution of the southern margin of Laurasia in the Black Sea region, *Int. Geol. Rev.*, 2015, vol. 57, no. 5–8, pp. 1051–1076.
https://doi.org/10.1080/00206814.2015.1010609

Okay, A.I., Tanzel, I., and Tüysüz, O., Obduction, subduction and collision as reflected in the Upper Cretaceous–Lower Eocene sedimentary record of Western Turkey, *Geol. Mag.*, 2001.
https://doi.org/10.1017/S0016756801005088

Okay, A.I., Sunal, G., Sherlock, S., Altiner, D., Tüysüz, O., Kylander–Clark, A.R.C., and Aygul, M., Early Cretaceous sedimentation and orogeny on the southern active margin of Eurasia: Central Pontides, Turkey, *Tectonics*, 2013.
https://doi.org/10.1002/tect.20077

Palcu, D.V., Patina, I.S., Sandric, I., et al., Late Miocene megalake regressions in Eurasia, *Sci. Rep.*, 2021, no. 11, p. 11471.

Patina, I.S. and Popov, S.V., Seismostratigraphy of regressive phases in the Maikop and Trkhan complexes on northern shelf of East Para-Tethys, in *Tektonika i geodinamika Zemnoi kory i mantii: fundamental'nye problemy–2023* (Tectonics and Geodynamics of the Earth's crust and Mantle: Fundamental Problems–2023), Moscow: GEOS, 2023, vol. 2, pp. 68–72.

Popov, S.V., Rögl, S., Rozanov, A.Y., Steininger, F.F., Shcherba, I.G., and Kovac, M., Lithological-palaeogeographic maps of the Paratethys, *Courier Forsch.–Inst. Senckenberg*, 2004, no. 250, p. 73.

Popov, S.V., Akhmet'ev, M.A., Lopatin, A.V., Bugrova, E.M., Sychevskaya, E.K., and Shcherba, I.G., *Paleogeografiya i biogeografiya basseinov Paratetisa* (Paleogeography and Biogeography of Basins in Para-Tethys), Moscow: Nauchn. Mir, 2009, part 1 (Late Eocene–Early Miocene).

Popov, S.V., Antipov, M.P., Zastrozhnov, A.S., Kurina, E.E., and Pinchuk, T.N., Sea-level fluctuations on the northern shelf of the Eastern Paratethys in the Oligocene–Neogene, *Stratigr. Geol. Correl.*, 2010, vol.18, no. 2, pp. 200–224.

Popov, D.V., Brovchenk, V.D., Nekrylov, N.A., et al., Removing a mask of alteration: geochemistry and age of the Karadag volcanic sequence in SE Crimea, *Lithos*, 2019, vol. 324, pp. 371–384.

Romanyuk, T.V., Kuznetsov, N.B., Rud'ko, S.V., Kolesnikova, A.A., Moskovskii, D.V., Dubenskii, A.S., Sheshukov, V.S., and Lyapunov, S.M., Isotopic-geochemical characteristics of the Carboniferous–Triassic magmatism in the Balck Sea region based on the study of detrital zircon grains from Jurassic coarse-clastic sequences of the Mountainous Crimea, *Geodinam. Tektonofiz.*, 2020, vol. 11, no. 3, pp. 453–473.
https://doi.org/10.5800/GT-2020-11-3-0486

Rubatto, D., Zircon: The metamorphic mineral, *Rev. Miner. Geochem.*, 2017, vol. 83(1), pp. 261–295.

Rud'ko, S.V., Kuznetsov, N.B., Romanyuk, T.V., and Belousova, E.A., Structure and the age of conglomerates in Mount Southern Demerdzhi based on the first U/Pb dating of detrital zircons (Upper Jurassic, Crimean Mountains), *Dokl. Earth Sci.*, 2018, vol. 483, no. 3, pp. 1423–1426.
https://doi.org/10.31857/S086956520003254-2

Rud'ko, S.V., Kuznetsov, N.B., Belousova, E.A., and Romanyuk T.V. Age, Hf-isotope systematics of detrital zircons and the sources of conglomerates in the southern Demerdzhi Mountain, Crimean Mountains, *Geotectonics*, 2019, no. 5, pp. 569–587.
https://doi.org/10.31857/S0016-853X2019536-61

Shanmugam, G., The turbidite–contourite–tidalite–baroclinite–hybridite problem: orthodoxy vs. empirical evidence behind the "Bouma Sequence", *J. Palaeogeogr.*, 2021, vol. 10, no. 9, pp. 1–32.
https://doi.org/10.1186/s42501-021-00085-1

Skublov, S.G., Berezin, A.V., and Berezhnaya, N.G., General relations in the trace-element composition of zircons from eclogites with implications for the age of eclogites in the Belomorian mobile belt, *Petrology*, 2012, vol. 20(5), pp. 427–449.

Sláma, J., Košler, J., Condon, D.J., Crowley, J.L., Gerdes, A., Hanchar, J.M., Horstwood, M.S.A., Morris, G.A., Nasdala, L., Norberg, N., Schaltegger, U., Schoene, B., Tubrett, M.N., and Whitehouse, M.J., Plešovice zircon—A new natural reference material for U–Pb and Hf isotopic microanalysis, *Geol. Mag.*, 2008, vol. 249, pp. 1–35.

Speijer, R.P., Pälike, H., Hollis, C.J., Hooker, J.J., and Ogg, J.G., Chapter 28 – the Paleogene Period, in *Geologic Time Scale*, 2020, vol. 2, pp. 1087–1140.
https://doi.org/10.1016/B978-0-12-824360-2.00028-0

Teipel, U., Eichhorn, R., Loth, G., Rohrmuller, J., Holl, R., and Kennedy, A., U–Pb SHRIMP and Nd isotopic data from the western Bohemian Massif (Bayerischer Wald, Germany): implications for Upper Vendian and Lower Ordovician magmatism, *Int. J. Earth Sci. (Geol. Rundsch.)*, 2004, vol. 93, pp. 782–801.

Tye, A.R., Niemi, N.A., Safarov, R.T., Kadirov, F.A., and Babayev, G.R., Sedimentary response to a collision orogeny recorded in detrital zircon provenance of Greater Caucasus foreland basin sediments, *Basin Res.*, 2021, vol. 33, no. 2, pp. 933–967.
https://doi.org/10.1111/BRE.12499

Vasey, D.A., Cowgill, E., Roeske, S.M., Niemi, N., Godoladze, T., Skhirtladze, I., and Godoladze, S., Evolution of the Greater Caucasus basement and formation of the Main Caucasus Thrust, Georgia, *Tectonics*, 2020, vol. 6, pp. 1–26.
https://doi.org/10.1029/2019TC005828

Vermeesch, P., How many grains are needed for a provenance study?, *Earth Planet. Sci. Lett.*, 2004, vol. 224, pp. 351–441.

Vermeesch, P., On the visualization of detrital age distributions, *Chem. Geol.*, 2012, vol. 312–313, pp. 190–194.

Vincent, S.J., Carter, A., Lavrishev, V.A., Rice, S.P., Barabadze, T.G., and Hovius, N., The exhumation of the western Greater Caucasus: a thermochronometric study, *Geol. Mag.*, 2011, vol. 148(1), pp. 1–21.
https://doi.org/10.1017/S0016756810000257

Wanless, V.D., Perfit, M.R., Ridley, W.I., Wallace, P.J., Grimes, C.B., and Klein, E.M., Volatile abundances and oxygen isotopes in basaltic to dacitic lavas on mid–ocean ridges: the role of assimilation at spreading centers, *Chem. Geol.*, 2011, vol. 287(1–2), pp. 54–65.
https://doi.org/10.1016/j.chemgeo.2011.05.017

Wiedenbeck, M., Allen, P., Corfu, F., Griffin, W.L., Meier, M., Oberli, F., Vonquadt, A., Roddick, J.C., and Speigel, W., Three natural zircon standards for U–Th–Pb, Lu–Hf, trace-element and REE analyses, *Geostand. Newsletter*, 1995, vol. 19, pp. 1–23.

Wiedenbeck, M., Hanchar, J.M., Peck, W.H., Sylvester, P., Valley, J., Whitehouse, M., Kronz, A., Morishita, Y., Nasdala, L., Fiebig, J., Franchi, I., Girard, J.P., Greenwood, R.C., Hinton, R., Kita, N., Mason, P.R.D., Norman, M., Ogasawara, M., Piccoli, R., Rhede, D., Satoh, H., Schulz–Dobrick, B., Skar, O., Spicuzza, M.J., Terada, K., Tindle, A., Togashi, S., Vennemann, T., Xie, Q., and Zheng, Y.F., Further characterization of the 91 500 zircon crystal, *Geostand. Geoanal. Res.*, 2004, vol. 28, pp. 9–39.

Wilhem, C. (Compiler), *Maps of the Callovian and Tithonian Paleogeography of the Caribbean, Atlantic, and Tethyan Realms: Facies and Environments*, Geol. Soc. Am. Digit. Map Chart Ser., 2014a, vol. 17, 3 sheets.

Wilhem, C., *Notes on Maps of the Callovian and Tithonian Paleogeography of the Caribbean, Atlantic, and Tethyan Realms: Facies and Environments*, *Geol. Soc. Am. Digit. Map Chart Ser.*, 2014b, vol. 17, p. 9.
https://doi.org/10.1130/2014.DMCH017

Yuan, H.-L., Gao, S., Dai, M.-N., Zong, C.-L., Gunther, D., Fontaine, G.H., Liu, X.-M., and Diwu, C.-R., Simultaneous determinations of U–Pb age, Hf isotopes and trace element compositions of zircon by excimer laser-ablation quadrupole and multiple-collector ICP-MS, *Chem. Geol.*, 2008, vol. 247, pp. 100–118.

Translated by D. Sakya

Publisher's Note. Pleiades Publishing remains neutral with regard to jurisdictional claims in published maps and institutional affiliations.